Asymmetric Neuroblast Divisions Producing Apoptotic Cells Require the Cytohesin GRP-1 in *Caenorhabditis elegans*

Jerome Teuliere,[1,2] Shaun Cordes,[1] Aakanksha Singhvi,[3] Karla Talavera, and Gian Garriga[4]
Department of Molecular and Cell Biology, Helen Wills Neuroscience Institute, University of California, Berkeley, California 94720

ABSTRACT Cytohesins are Arf guanine nucleotide exchange factors (GEFs) that regulate membrane trafficking and actin cytoskeletal dynamics. We report here that GRP-1, the sole *Caenorhabditis elegans* cytohesin, controls the asymmetric divisions of certain neuroblasts that divide to produce a larger neuronal precursor or neuron and a smaller cell fated to die. In the Q neuroblast lineage, loss of GRP-1 led to the production of daughter cells that are more similar in size and to the transformation of the normally apoptotic daughter into its sister, resulting in the production of extra neurons. Genetic interactions suggest that GRP-1 functions with the previously described Arf GAP CNT-2 and two other Arf GEFs, EFA-6 and BRIS-1, to regulate the activity of Arf GTPases. In agreement with this model, we show that GRP-1's GEF activity, mediated by its SEC7 domain, is necessary for the posterior Q cell (Q.p) neuroblast division and that both GRP-1 and CNT-2 function in the Q.posterior Q daughter cell (Q.p) to promote its asymmetry. Although functional GFP-tagged GRP-1 proteins localized to the nucleus, the extra cell defects were rescued by targeting the Arf GEF activity of GRP-1 to the plasma membrane, suggesting that GRP-1 acts at the plasma membrane. The detection of endogenous GRP-1 protein at cytokinesis remnants, or midbodies, is consistent with GRP-1 functioning at the plasma membrane and perhaps at the cytokinetic furrow to promote the asymmetry of the divisions that require its function.

METAZOAN development relies on the coordinated behavior of individual cells that either adopt morphogenetic behaviors such as proliferation, migration, adhesion, and differentiation, or die at precise times and places. Despite extensive characterization of the molecular mechanisms associated with the execution of programmed cell death (PCD) during development, less is known about how a given cell chooses to live or die. PCD execution often relies on the activation of versatile proteases, the caspases, by an evolutionarily conserved molecular cascade. In the nematode *Caenorhabditis elegans*, somatic PCD is largely determined by asymmetric cell divisions that produce a surviving daughter cell and a daughter cell fated to die (Frank *et al.* 2005; Cordes *et al.* 2006; Hatzold and Conradt 2008; Ou *et al.* 2010; Singhvi *et al.* 2011). The invariant lineage that produces these dying cells makes *C. elegans* a powerful system to explore the mechanisms involved in PCD specification.

Although several studies point to the cell-specific transcriptional control of EGL-1, a BH3-only protein that can activate the caspase cascade, as a mechanism of PCD specification (Potts and Cameron 2011), other data suggest that daughter cell-size asymmetry regulates PCD (Frank *et al.* 2005; Cordes *et al.* 2006; Hatzold and Conradt 2008; Ou *et al.* 2010; Singhvi *et al.* 2011). Indeed, *C. elegans* divisions that generate dying cells are generally asymmetric, producing a larger surviving daughter and a smaller daughter fated to die. Several mutants affecting this size difference also perturb PCD specification, leading to the survival of both daughter cells.

The ADP-ribosylation factor (Arf) GTPase-activating protein (GAP) CNT-2 and two *C. elegans* Arf GTPases that function with CNT-2 were previously shown to control cell size and cell death in asymmetric neuroblast divisions by an unknown mechanism (Singhvi *et al.* 2011). Arfs are small GTPases that regulate secretory and endocytic pathways,

doi: 10.1534/genetics.114.167189
Manuscript received June 10, 2014; accepted for publication July 10, 2014; published Early Online July 21, 2014.
Supporting information is available online at http://www.genetics.org/lookup/suppl/doi:10.1534/genetics.114.167189/-/DC1.
[1]These authors contributed equally to this work.
[2]Present address: Complete Genomics, Inc., Mountain View, CA 94043.
[3]Present address: Laboratory of Developmental Genetics, Rockefeller University, 1230 York Ave., New York, NY 10065.
[4]Corresponding author: 401 Barker Hall, University of California, Berkeley, CA 94720. E-mail: garriga@berkeley.edu

as well as the actin cytoskeleton (Donaldson and Jackson 2011). Arfs fall into three classes based on sequence homology: class I (Arf1-3), class II (Arf4-5), and the more divergent class III (Arf6) (Kahn *et al.* 2006). Class I and II Arfs localize to Golgi and endosomal compartments and are required for protein trafficking in the secretory and endocytic pathways. Arf6, by contrast, localizes to the plasma membrane and to endosomes and has been shown to regulate events near the cell surface, including endocytosis, exocytosis, and cortical actin structure (Donaldson and Jackson 2011). Arfs exist in active (GTP bound) and inactive (GDP bound) states that are controlled by accessory proteins. Guanine nucleotide exchange factors (GEFs) facilitate GDP release and GTP binding, and GAPs like CNT-2 stimulate hydrolysis of GTP to GDP. Arf-GTP can recruit coatomer proteins and initiate the formation of membrane vesicles. The cycling between GDP- and GTP-bound states is necessary for Arfs to regulate vesicle budding (Kreis *et al.* 1995).

In this report, we describe the involvement of **G**eneral **R**eceptor for **P**hosphoinositides-**1** (GRP-1), an Arf GEF of the cytohesin family, in asymmetric neuroblast divisions and PCD specification. Cytohesins contain an N-terminal coiled-coil (CC) domain, a central SEC7 domain that contains ARF GEF activity, and a C-terminal pleckstrin-homology (PH) domain (reviewed in Jackson *et al.* 2000; Moss and Vaughan 2002). Cytohesins have been implicated in regulating signal transduction, actin cytoskeletal dynamics, protein trafficking in the exocytic and endocytic pathways, and cell adhesion (Jackson *et al.* 2000; Moss and Vaughan 2002; Kolanus 2007).

Since most of the previous studies of cytohesins focused exclusively on assays conducted in cultured cell lines, the functions of these molecules during animal development are still poorly understood. Here we report that GRP-1 possibly regulates multiple *C. elegans* Arfs together with the previously described Arf GAP CNT-2. We show that both GRP-1 and CNT-2 act autonomously in dividing neuroblasts that produce a dying daughter. In the absence of GRP-1 function, the apoptotic daughters of these neuroblasts are transformed into their sisters, resulting in the production of extra neurons. Human cytohesins can functionally substitute for GRP-1 to regulate neuroblast divisions. We also provide evidence that other Arf GEFs, acting in parallel to GRP-1, function in these divisions. Surprisingly, we find GFP-tagged GRP-1 localized to the nucleus due to the presence of a nuclear localization signal in the GRP-1 CC domain. Targeting the Arf GEF domain to different cellular compartments, however, suggests that it acts at the plasma membrane. Supporting this model, we found that endogenous GRP-1 is associated with midbodies, cytokinesis remnants of dividing cells.

Materials and Methods

C. elegans genetics

General handling and culture of nematodes were performed as previously described (Brenner 1974). The N2 Bristol line was used as wild type, and experiments were performed at 20° unless otherwise noted. The following mutations and integrated arrays were used:

LG I. *ynIs45* [*Pflp-15*::*gfp*] (Kim and Li 2004), *zdIs5* [*mec-4*::*gfp*] (Clark and Chiu 2003).

LG II. *rrf-3(pk1426)* (Simmer *et al.* 2002), MosSCI transgenes integrated at the ttTi5605 site (see Table 1) (Frøkjær-Jensen *et al.* 2008), *gmIs20* [*hlh-14*::*gfp*] (Frank *et al.* 2003), *ynIs25* [*Pflp-12*::*gfp*] (Li *et al.* 1999; Kim and Li 2004).

LG III. *ced-4(n1182)* (Ellis and Horvitz 1986), *arf-1.2(ok796)* (Singhvi *et al.* 2011), *grp-1(gm350*, *gk402275)* (this study), *grp-1(tm1956)* (Denning *et al.* 2012), *lon-1(e185)* (Brenner 1974), *unc-32(e189)* (Brenner 1974), *cnt-2(gm377)* (Singhvi *et al.* 2011), *unc-119(ed3)* (Maduro and Pilgrim 1995), *gmIs12* [*Psrb-6*::*gfp*] (Hawkins *et al.* 2005), *rdvIs1* [*Pegl-17*::*mCherry:his-24* + *Pegl-17*::*myristoylated mCherry* + *pRF4*] (Ou *et al.* 2010).

LG IV. *eri-1(mg366)* (Kennedy *et al.* 2004), *pig-1(gm301)* (Cordes *et al.* 2006), *bris-1(gk592726)* (this study), *arf-3(tm1877)* (this study), *efa-6(tm3124)* (O'Rourke *et al.* 2010), *dpy-20(e1282ts)* (Brenner 1974), *ced-3(n717*, *n2436)* (Ellis and Horvitz 1986; Shaham *et al.* 1999), *unc-30(e191)* (Brenner 1974), *arf-6(tm1447)* (Singhvi *et al.* 2011), *mgIs71* [*tph-1*::*gfp*] (Bülow and Hobert 2004).

LG V. *egl-1(n1084 n3082)* (Conradt and Horvitz 1998), *ayIs9* [*Pegl-17*::*gfp*] (Branda and Stern 2000), *gmIs65* [*Psra-6*::*mCherry*, *Ptph-1*::*gfp*] (a kind gift from Richard Ikegami).

LG X. *gmIs81* [*Pmec-4*::*mCherry, Pflp-12*::*EBFP2, Pgcy-32*::*gfp, Pegl-17*::*gfp*] (Gurling *et al.* 2014).

Detection of specific neurons

All neurons were detected with chromosomally integrated transcriptional reporters that express GFP under control of the indicated *C. elegans* promoter. The ALM, AVM, PVM, and PLM neurons were detected using the reporter *zdIs5* [*mec-4*::*gfp*]. The SDQ neurons were detected using the reporter *ynIs25* [*flp-12*::*gfp*]. The PHB neurons were visualized in L1 larvae using *gmIs12* [*Psrb-6*::*gfp*], which is expressed both in PHB and the adjacent PHA neurons. The PHA and I2 neurons were detected using the reporter *ynIs45* [*flp-15*::*gfp*]. Reducing *grp-1* activity does not alter the number of PHA neurons in *ced-3(+)* or *ced-3(n717)* backgrounds (data not shown), indicating that the extra neurons observed using *gmIs12* are PHBs. The HSN neurons were detected using *mgIs71* [*tph-1*::*gfp*] (Sze *et al.* 2002; Bülow and Hobert 2004), and by immunostaining adult hermaphrodites with rabbit antiserotonin antibodies as previously described (Garriga *et al.* 1993). The A/PQR neurons were detected using the *gmIs81* [*Pgcy-32*::*gfp*] reporter. The NSM neurons were scored using the *gmIs65* [*Ptph-1*::*gfp*] reporter.

Table 1 A/PVM phenotypes of RNAi-treated animals and mutants

	Gene	% extra A/PVMs[a]	*n*
	Control/L4440	4	457
	grp-1/ K06H7.4[b]	72[c]	463
	cnt-2/Y39A1A.15[d]	49[c]	218
arfs and *arf*-related genes (RNAi)	*arf-1.2*/ B0336.2[b]	41[c]	51
	arf-1.2/ B0336.2[e]	49[c]	76
	arf-3/ F57H12.1[b]	28[f]	80
	arf-6/ Y116A8C.12[e]	30[c]	98
	arf-1.1/ F45E4.1[e]	10[f]	171
	arl-1/ F54C9.10[e]	8[g]	135
	evl-20/arl-2/ F22B5.1[b]	5[h]	130
	arl-3/ ^{19}FH8.3[b]	6[h]	142
	arc-1/arl-4/ ZK1320.6[e]	10[f]	122
	arl-5/ ZK632.8[b]	6[h]	130
	arl-6/ C38D4.8[d]	7[h]	150
	arl-7/ F20D1.5 (pseudogene)[b]	6[h]	132
	arl-8/ Y57G11C.13[e]	5[h]	131
	arl-13/ Y37E3.5[d]	5[c]	159
	Y54E10BR.2[e]	4[h]	131
	sar-1/ ZK180.4[b]	10[g]	70
arfs (mutants)			
	arf-3(tm1877, m+)	0	107
	ced-4(n1162)	12	240
	ced-4(n1162); arf-3(tm1877, m+)	1	168
arls (mutants)	*ced-3(n717)*	12	445
	ced-4(n1162)	12	240
	evl-20(ar103); ced-3(n717)	10[i]	209
	arl-5(ok2407); ced-3(n717)	11[i]	180
	ced-4(n1162); arl-8(wy271)	15[i]	218

[a] Extra A/PVMs in the RNAi experiments were scored in a *zdIs5; rrf-3; ced-3(n2436)* strain.
[b] RNAi clones were from Kamath *et al.* (2001).
[c] Significantly different from L4440 control $P < 0.001$.
[d] RNAi clones were constructed for this study.
[e] RNAi clones were from Rual *et al.* (2004).
[f] Significantly different from L4440 control $P < 0.02$.
[g] Significantly different from L4440 control $P < 0.05$.
[h] Not significantly different from L4440 control.
[i] Not significantly different from *ced-3* or *ced-4* control.

Isolation and cloning of grp-1(gm350)

We mutagenized *zdIs5* [*mec-4*::*gfp*]; *ced-3(n2436)* hermaphrodites with 50 mM ethylmethylsulfonate and screened F_2's for mutations that strongly enhanced the penetrance of extra AVMs, PVMs, and PLMs above the level observed in *ced-3(n2436)* (data not shown). *grp-1(gm350)*; *ced-3(n2436)* had a high penetrance of extra AVMs, PVMs, PLMs, and HSNs.

To map *gm350*, we first separated the mutation from *ced-3(n2436)* and then used single-nucleotide polymorphism (SNP) mapping to position *gm350* between snp_F27B3[1] and pkP3049 on LG III (Wicks *et al.* 2001), a 180-kb region containing ~45 open reading frames (ORFs).

To determine which of the 45 ORFs was likely to be mutated in *gm350* mutants, we systematically inactivated all but two of the ORFs by RNA-mediated interference (RNAi) in *zdIs5*; *ced-3(n2436)* hermaphrodites (Timmons and Fire 1998; Kamath *et al.* 2001). The *grp-1* ORF, K06H7.4, was the only gene in this region that phenocopied the original *zdIs5*; *gm350*; *ced-3(n2436)* mutant when inactivated by RNAi (Supporting Information, Figure S1). To determine whether the *gm350* lesion was located in *grp-1*, we sequenced the ORF in *gm350* mutants and identified a single nonsense mutation (Figure 1A).

Protein sequence analysis

Sequence alignments and dendrograms were generated using ClustalW2 (https://www.ebi.ac.uk/Tools/msa/clustalw2/). The GenBank accession numbers for sequences used in phylogenetic analyses are: *C. elegans* GRP-1, NP_498764; *Drosophila melanogaster* steppke, NP_610120; *Homo sapiens* CYTH1, NP_004753.1, CYTH2, NP_059431.1, CYTH3, NP_004218.1, CYTH4, NP_037517.1; and *Mus musculus* Cyth1, NP_035310.2, Cyth2, NP_035311.1, Cyth3, NP_035312.2, Cyth4, NP_082471.2.

RNAi

RNAi was performed by feeding worms individual bacterial clones as described (Timmons and Fire 1998). Clones were from the libraries constructed in the Ahringer lab (Timmons and Fire 1998; Kamath *et al.* 2001) or the Vidal lab (Rual *et al.* 2004), or were generated for this study as indicated. The negative control used in these experiments was a clone containing

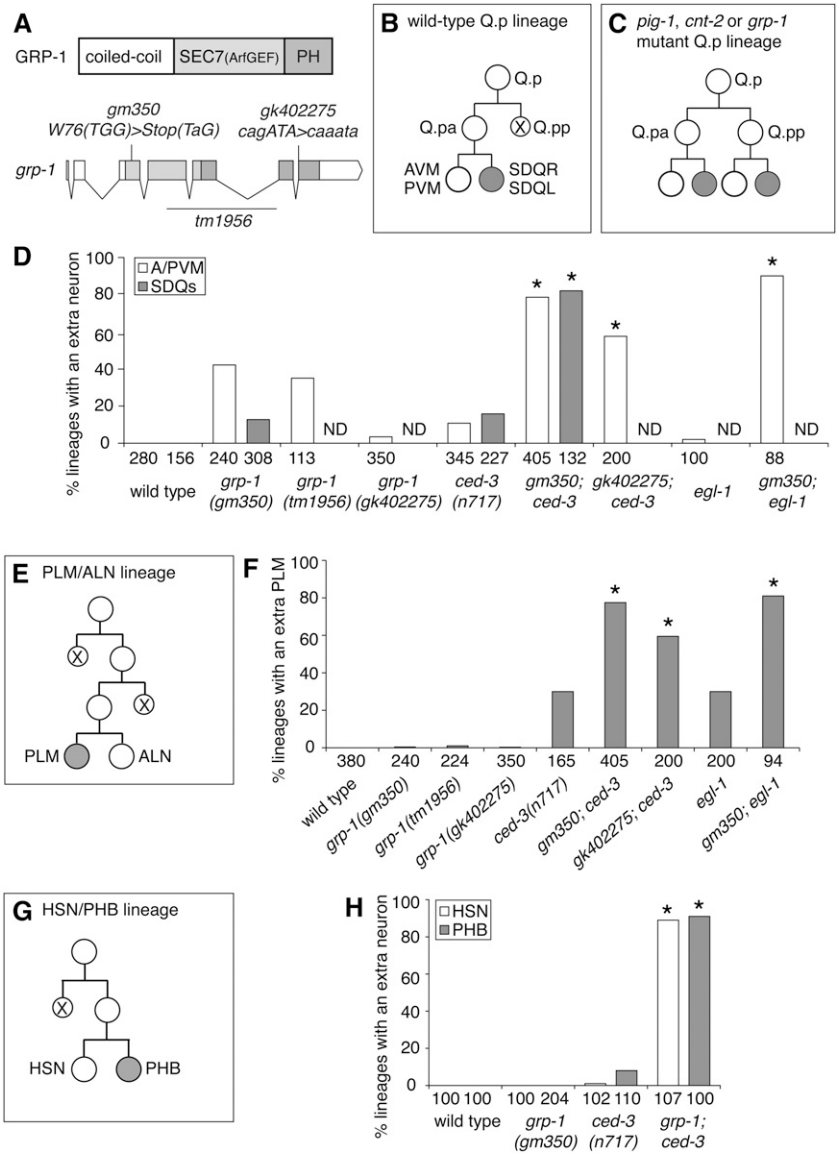

Figure 1 The gene *grp-1* regulates apoptosis in multiple neuroblast lineages. (A) Schematic diagram of the GRP-1 domain structure and the *grp-1* genomic structure and mutations. *grp-1(gm350)* is a nonsense mutation at the beginning of the SEC7(Arf GEF) domain (W76TaGStop). The *grp-1(tm1956)* mutation is a deletion that removes part of the SEC7 and PH domains and shifts the reading frame. The *grp-1(gk402275)* mutation is a 3′ splice site mutation that changes the last nucleotide G of the last intron to A, which is predicted to disrupt RNA splicing and result in an altered pleckstrin homology (PH) domain. (B) The wild-type Q.p neuroblast lineage produces two neuron types (A/PVMs and SDQs) and a dying cell (Q.pp). (C) The Q.p divisions of *pig-1*, *cnt-2*, and *grp-1* mutants produce daughters that are more equivalent in size, and the posterior daughter cell can behave like its mitotic sister cell, surviving, dividing, and producing extra neurons with A/PVM and SDQ fates. (E and G) The wild-type PLM/ALN (E) and HSN/PHB (F) neuroblast lineages each produce two neuron types and dying cells. (D and F) The *grp-1* mutations interact synergistically with *ced-3* and *egl-1* mutations to produce extra A/PVM and SDQ neurons in the Q.p lineage (D) and extra PLM neurons (F). (H) *grp-1(gm350)* and *ced-3 (n717)* mutations interact synergistically to produce extra HSN and PHB neurons. In all lineage diagrams, the anterior cell is to the left, and apoptotic cells are indicated by an "X." All neurons were scored using cell-specific GFP reporters as described in *Materials and Methods*. The number of lineages scored per genotype is shown under each bar. ND, not determined. $^*P < 0.0001$ in comparison to either single mutant.

empty vector (L4440) in the bacterial host HT115 (Timmons and Fire 1998), the same host used for the RNAi feeding experiments. A clone was constructed to target the SEC7 protein-encoding gene *Y106G6G.2* (Supporting Information) and introduced into HT115 bacteria, the same approach used to generate the clones from the Arhinger and Vidal labs' libraries (Kamath *et al.* 2001; Rual *et al.* 2004).

Analysis of neuroblast daughters size and the number of cells produced by Q.p

For Q.p and the anterior Q (Q.a) daughter cell-size measurements, anterior and posterior daughter cell areas were measured in triplicate using ImageJ, on the left side of L1 larvae carrying the Q lineage markers *rdvIs1* [*Pegl-17*::*mCherry:his-24* + *Pegl-17*::*myristoylated mCherry*] (Q.p daughters) or *gmIs81* [*Pegl-17*::*gfp*] (Q.a daughters). The size ratio was calculated using the average area values from the three measurements. We only measured the relative sizes of the daughter cells when the posterior daughter cell of Q.p (Q.pp) or the anterior daughter cell of Q.a (Q.aa) did not appear apoptotic: they were not rounded and were still attached to their respective sister.

The persistence of the *rdvIs1* mCherry signal in Q.p descendants allowed us to determine the final number of surviving cells in the Q.p lineage progeny before expression was lost. We only scored cells that were not rounded and were located at the position where Q.p had been. The *rdvIs1* marker also labels Q.a and its daughters, which could make the identification of Q.p progeny ambiguous. Since the Q.aa cell dies before the Q.pp cell, we only analyzed lineages where we could identify the Q.aa dying cell and its surviving sister unambiguously by their positions, and thus, exclude them from the scoring.

Plasmid construction and transgenics

The detail of DNA manipulations is presented in Supporting Information. Transgenic lines were generated by injecting

plasmid DNA into the syncytial hermaphrodite gonad. MosSCI lines were generated as described by injecting the EG6699 *ttTi5605*, *unc-119(ed3)* mutants (Frøkjær-Jensen *et al.* 2014). All transgenes used in this study are described in Table S1.

Analysis of grp-1 cell autonomy

For the mosaic analysis, *zdIs5*; *grp-1(gm350)* hermaphrodites were injected with plasmid bGG836 [*grp-1(+)*] and the cell-autonomous marker *Pdpy-30*::*NLS*::*DsRed2*. Animals carrying the resulting extrachromosomal arrays (*gmEx353-5*; Table S1) were rescued for the Grp-1 A/PVM phenotype (data not shown). Extrachromosomal arrays are mitotically unstable, and thus animals carrying these arrays are mosaic, frequently having lost the array from one or more lineages. We screened *zdIs5*; *grp-1*; *gmEx353* mosaic animals for those with extra A/PVMs and then determined which lineages had lost the array by scoring nuclear DsRed2 expression.

For *grp-1* rescue using the *mab-5* promoter assay, *zdIs5* [*mec-4*::*gfp*]; *grp-1(gm350)* mutants were injected with *Pmab-5*::*grp-1*::*gfp* and the cell-autonomous marker *Pdpy-30*::*NLS*::*DsRed2*. The *Pdpy-30*::*NLS*::*DsRed2* plasmid drives ubiquitous expression of nuclear-localized DsRed2 and allowed us to unambiguously determine which cells in mosaic animals contained the extrachromosomal array. As a negative control in all experiments, animals carrying the extrachromosomal array were compared to their siblings on the same plate that had lost the array. Rescue of Grp-1 phenotypes was assessed by determining whether *grp-1* mutants that did not express *Pmab-5*::*grp-1*::*gfp* had a significantly higher percentage of sides with an extra cell compared to transgenic animals where the array was present in the A/PVM neurons.

The *arf-6* rescue experiment was performed with the integrated MosSCI transgene *gmSi33* (Table S1) introduced by crosses into the *ced-4*; *arf-6* double mutant.

For the *unc-86* promoter assay, integrated MosSCI transgenes [*Punc-86*::*grp-1*::*gfp*] and [*Punc-86*::*cnt-2b*::*gfp*] (Table S1) were crossed into *zdIs5* [*mec-4*::*gfp*]; *grp-1(gm350)* or *zdIs5* [*mec-4*::*gfp*]; *cnt-2(gm377)* mutants, respectively.

Statistical analysis

Statistical analysis was performed using the two-sample *Z*-test for proportions for extra cell scoring and the Mann–Whitney *U*-test for cell size ratios.

Immunofluorescence

Adults and larvae were removed from starved plates by washing, leaving embryos that were collected, fixed, and permeabilized as described (Guenther and Garriga 1996). Rabbit anti-GRP-1 antibodies (Covance, raised against a 29-amino-acid peptide corresponding to GRP-1 C-terminal sequence DEDMRSWINAISRMMAPQQHLLARPKSTH) were diluted 1:1000 in PBST-A (1× PBS, 1% BSA, 0.5% Triton X-100, 0.05% NaN3, 1 mM EDTA), and the dilution was incubated overnight at room temperature with fixed embryos. To detect NMY-2::GFP and ZEN-4::GFP fusions, a chicken anti-GFP antibody diluted 1/500 was added (Molecular Probes). After washing, the embryos were rocked 4 hr at room temperature in Alexa 568 goat anti-rabbit antisera and, when needed, Alexa 488 anti-chicken antisera diluted 1:100 in PBST-A (Molecular Probes). After washing three times and DAPI counterstaining, embryos were mounted in Vectashield Mounting Medium (Vector Laboratories). Pictures were obtained from a Hamamatsu ORCA-ER digital camera attached to a Zeiss Axioskop2 microscope using Openlab software.

Confocal microscopy

For detection of GRP-1 fusion proteins, live animals were mounted in 3 μl of a solution containing 33 μM sodium azide in M9 minimal medium on an agarose pad. Confocal microscopy of live and fixed immunostained animals was performed on a Leica TCS NT confocal microscope. Projections of confocal images were generated with ImageJ software (http://imagej.nih.gov/ij/) using the standard deviation method. Images were prepared for publication using Adobe Photoshop.

Time-lapse images of the Q.p division were acquired as described (Singhvi *et al.* 2011). *rdvIs1* and *Pmab-5*::*gfp*::*efa-6* images were acquired with the 561- and 488-nm rays of a Marianas spinning disc confocal microscope (Intelligent Imaging Innovations) using a ×100 1.4-NA objective and the SlideBook software.

Results

Isolation of the grp-1(gm350) mutant

A subset of *C. elegans* neurons are generated by neuroblast asymmetric divisions that produce a daughter cell that dies and a neuron or neuronal precursor. The kinase PIG-1 and the Arf GAP CNT-2 have been shown to regulate the cell death decision in many of these divisions (Cordes *et al.* 2006; Ou *et al.* 2010; Singhvi *et al.* 2011; Hirose and Horvitz 2013). To identify additional genes that might function with *pig-1* or *cnt-2*, we screened for mutants with extra neurons that expressed the *Pmec-4*::*gfp* transgene *zdIs5* and are located in the positions normally occupied by the AVM and PVM neurons. The posterior daughter of the Q neuroblast, Q.p, divides to produce a posterior cell that dies and an anterior precursor that divides to produce the A/PVM and SDQ neurons, resulting in an AVM and SDQ on the right side and a PVM and SDQ on the left (Figure 1B). Loss of PIG-1 or CNT-2 often results in a posterior Q.p daughter cell that survives and adopts the fate of its sister, resulting in the production of extra neurons (Figure 1C) (Cordes *et al.* 2006; Singhvi *et al.* 2011). Extra neurons that express *zdIs5* usually have axons that project ventrally, similar to the AVM and PVM axons. When there is more than one neuron on a side that expresses *zdIs5*, we refer to the additional neurons as extra A/PVMs. Since mutations in the caspase gene

ced-3 strongly enhance the phenotypes of *pig-1* mutants, we used *ced-3(n2436)*, a partial loss-of-function mutation, to sensitize the background of our screen. We isolated the *gm350* mutant on the basis of this extra A/PVM defect and found that it also displayed extra PLMs and HSNs, similar to *pig-1* and *cnt-2* mutants (Figure 1, B–H and Figure S1A). We mapped the *gm350* lesion to the gene *grp-1*. A second allele of *grp-1*, *tm1956*, was obtained from the National Biosource Project (http://www.shigen.nig.ac.jp/c.elegans/index.jsp) and it caused a similar extra A/PVM phenotype (Figure 1, A and D). A third, hypomorphic allele, *grp-1(gk402275)*, was identified by the Million Mutation Project (http://genome.sfu.ca/mmp/) and it caused milder defects (Figure 1, A and D).

Several observations suggest that the phenotypes observed in these mutants were caused by a loss of GRP-1 activity. First, meiotic mapping placed *gm350* close to the *grp-1* locus, and DNA sequencing confirmed the presence of a nonsense mutation in the *grp-1* ORF (*Materials and Methods* and Figure 1A). Second, RNAi of the *grp-1* locus generated phenotypes similar to those produced by the *gm350* and *tm1956* alleles (Figure 1, D, F, and H and Figure S1B). Third, the two strong alleles are predicted to impair GRP-1 function (see below). Fourth, complementation tests showed *tm1956* and *gk402275* failed to complement *gm350* (data not shown). Finally, expressing a *grp-1* cDNA from various *C. elegans* promoters rescued the *grp-1(gm350)* mutant phenotypes (see below).

GRP-1 is a member of the cytohesin family of ARF GEFs: GRP-1 is the sole *C. elegans* member of the cytohesin family of Arf GEFs. Like vertebrate cytohesins, nematode GRP-1 contains an N-terminal CC domain, a central SEC7 domain that contains Arf GEF activity, and a C-terminal PH domain (Figure 1A). *C. elegans* GRP-1 and all four human cytohesins are 38.5% (CYTH4) to 41.7% (CYTH3) identical over the full length of the protein, and >60% similar with a high level of conservation in all three domains. The *grp-1(gm350)* mutation isolated in our genetic screen is a nonsense mutation (W76ochre) located at the beginning of the SEC7 domain. The *grp-1(tm1956)* mutation, a 983-bp deletion and single-bp insertion, removes the second half of the SEC7 domain and the first part of the PH domain and is predicted to introduce a shift in the reading frame. The *grp-1(gk402275)* mutation is a 3′ splice site mutation in the last intron of *grp-1* (Figure 1A). Because the proteins encoded by both *gm350* and *tm1956* mutants are predicted to lack intact SEC7 and PH domains, and because expression of the CC domain alone cannot rescue the mutant phenotypes of *grp-1* mutants (see below), we infer that *gm350* and *tm1956* severely reduce or eliminate *grp-1* function.

grp-1 functions in parallel to the programmed cell death pathway in multiple neuroblast lineages: The *grp-1(gm350)*; *ced-3(n2436)* mutant isolated from our sensitized screen had extra AVM, PVM, PLM, and HSN neurons (Figure S1A). To characterize the *grp-1* phenotype in the absence of other mutations, we scored *grp-1* mutants in a wild-type *ced-3* background. These mutants had extra neurons derived from the Q.p neuroblast, but had few extra neurons derived from the HSN/PHB lineages (Figure 1, D and H) in comparison to the original *grp-1*; *ced-3(n2436)* mutant strain isolated from our screen. An examination of animals with mutations in *grp-1* and strong mutations in the proapoptotic genes *ced-3* or *egl-1* supports the hypothesis that *grp-1* and *ced-3* mutations interact synergistically and demonstrate that *grp-1* also regulates the number of PHB neurons (Figure 1, D, F, and H). Finally, we observed that the *grp-1(gm350)* mutant had weak extra neuron defects in other neuroblast lineages such as the Q.a lineage (1.8% extra A/PQR neurons, $n = 168$), the I2 lineage (3% extra I2 neurons, $n = 100$), and the NSM lineage (3.6% extra NSM neurons, $n = 302$). Together, these observations indicate that *grp-1*, like *pig-1*, functions partly in parallel to the PCD execution pathway to regulate the asymmetric divisions of certain neuroblasts. All subsequent experiments that involve a *grp-1* mutant were carried out with the *gm350* allele.

GFP::GRP-1 fusions localized to nuclei and rescued the grp-1 mutant: To characterize the GRP-1 expression pattern and subcellular localization, we introduced a translational GFP::GRP-1 cDNA fusion expressed under the control of the *grp-1* promoter into *grp-1* mutant worms (Figure 2). We observed that GFP::GRP-1 transgene expression was widespread in somatic cells of embryos, larvae, and adults, and was concentrated in the nuclei of interphase cells (Figure 2, A–C and data not shown). Since vertebrate cytohesins localize to the cytoplasm and the plasma membrane, the GFP::GRP-1 enrichment in nuclei was unexpected. Two independently generated transgenes generated the same expression pattern, were able to rescue the extra A/PVM phenotype caused by the *grp-1* mutation (Figure 2D), and did not induce any extra cell phenotype in wild-type *grp-1* background (data not shown).

Human cytohesins can functionally substitute for nematode GRP-1: To test whether human cytohesins can provide GRP-1 function, we expressed GFP fusions to cDNAs of three human family members [cytohesin-1 (CYTH1), cytohesin-2 (CYTH2), and cytohesin-4 (CYTH4)] in *C. elegans*, examined the localization of these fusions in embryos, and determined whether they could rescue the *grp-1* mutant A/PVM phenotype (Figure S2). All of the cytohesin transgenes were expressed from the *dpy-30* promoter, which drives widespread expression (Hsu *et al.* 1995). We found that the CYTH1 and CYTH2 fusions localized to the plasma membrane and that CYTH1 also localized weakly to nuclei, but we did not observe any specific localization for the CYTH4 fusion (Figure S2, C–E′). All three fusions rescued the extra-A/PVM phenotype of *grp-1* mutants (Figure S2F), supporting the hypothesis that GRP-1 is a cytohesin ortholog. The ability of both membrane-localized CYTH2 and nuclear GRP-1 to rescue the *grp-1* mutant phenotype raises the issue of where GRP-1 normally functions in the cell.

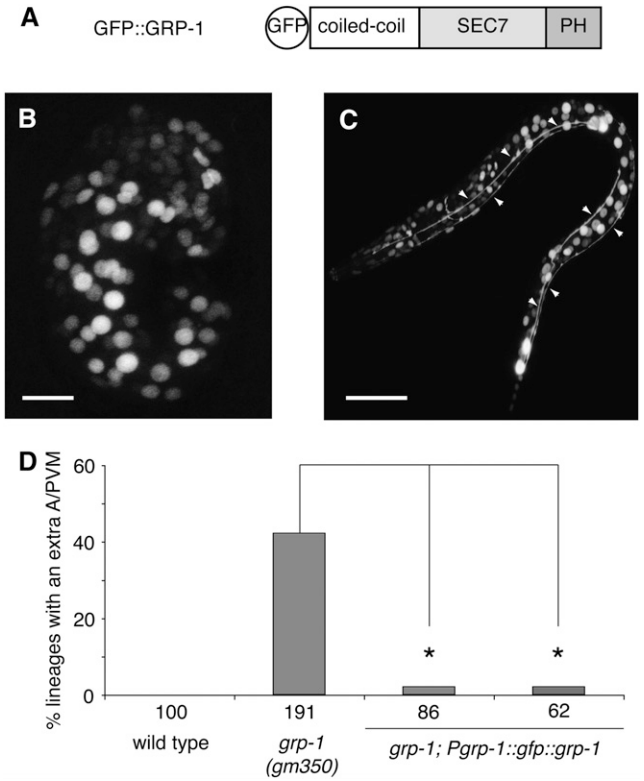

Figure 2 Functional GFP::GRP-1 localizes to nuclei. (A) Diagram of the GFP::GRP-1 construct. Expression of this GFP fusion was driven off the *grp-1* promoter. (B and C) Confocal projections of *zdIs5* [*mec-4*::*gfp*]; *grp-1(gm350)*; *Pgrp-1*::*gfp*::*grp-1* in an embryo (B) and a L1 larva (C). Arrows mark the ALM and PLM processes labeled by the *zdIs5* transgene. Bar, 10 μm (B) and 20 μm (C). (D) Expression of *Pgrp-1*::*gfp*::*grp-1* from two independently isolated extrachromosomal arrays rescued the A/PVM phenotype of *grp-1* mutants. The number of lineages scored per genotype is shown under each bar. $*P < 0.0001$.

GRP-1 may function in an Arf GTPase cycle with CNT-2: The CNT-2 GAP domain was previously shown to be required for its function in asymmetric neuroblast divisions (Singhvi *et al.* 2011). As both CNT-2 and GRP-1 are predicted to regulate Arf GTPases, they may be components of the same Arf cycle. In agreement with this model, the *grp-1 cnt-2* double mutant had the same penetrance of extra-A/PVM neurons as the *cnt-2* single mutant, suggesting that *grp-1* and *cnt-2* act in the same genetic pathway (Figure 3). Since the completion of the Arf GTP-bound to GDP-bound cycling is thought to be essential for vesicular budding (Kreis *et al.* 1995), we expected to observe similar defects when the cycle is compromised by disrupting the Arf GAP. The lower penetrance of the *grp-1* mutants, however, suggests that CNT-2 has other functions or acts with Arf GEFs other than GRP-1 (Figure 3).

Additional Arf GEF proteins regulate the Q.p division: To test whether other Arf GEF proteins may compensate for *grp-1* loss, we performed an RNAi *grp-1* enhancer screen using RNAi clones targeting other SEC7 domain-containing proteins of *C. elegans*. We found that knocking down the function of two Arf GEFs, EFA-6 and M02B7.5, which we name BRIS-1 for its homologs **BR**AG/**I**QSEC/**S**chizo, were able to enhance the *grp-1* A/PVM phenotype, but did not induce a phenotype in animals that were wild type for *grp-1* (Figure S3). Using *efa-6* and *bris-1* mutations, we confirmed this enhancer effect in the *grp-1* mutant (Figure 3). Taken together, our genetic data are consistent with a model where GRP-1 and these other Arf GEFs function with CNT-2 to regulate the Q.p asymmetric division. Our findings do not distinguish between models where the Arf GEFs act together with CNT-2 to regulate a single membrane trafficking event or where they function with CNT-2 in separate events.

ARF-6 acts with GRP-1 to regulate the Q.p division: To determine which Arfs are regulated by GRP-1, we analyzed the *arf-1.2*, *arf-3*, and *arf-6* genes, which encode the sole *C. elegans* orthologs of classes I, II, and III Arfs, respectively (Li *et al.* 2004). Two Arf GTPases, *arf-1.2* and *arf-6*, have been previously implicated in the regulation of the Q.p neuroblast asymmetric division (Singhvi *et al.* 2011). Whereas single Arf mutants have subtle phenotypes and only generate extra cells in a sensitized *ced* mutant background (Singhvi *et al.* 2011), the *arf-1.2*; *arf-6* double mutant displayed a synthetic A/PVM phenotype, suggesting that the two Arfs can compensate for each other's loss (Figure 3). However, the penetrance of the defects in the double Arf mutant was significantly lower than the defects observed in *cnt-2* ($P < 0.0001$) and *grp-1* ($P < 0.005$) mutants, suggesting that additional Arfs or Arf-like (Arl) GTPases regulate the Q.p division (Figure 3).

We used RNAi to test the role of each of the *C. elegans* Arf and Arl genes in the Q.p division by scoring the number of A/PVMs in a *rrf-3*; *ced-3(n2436)* mutant background (Table 1). The *rrf-3* mutation sensitizes the animals to the effects of RNAi (Simmer *et al.* 2002), and the *ced-3(n2436)* mutation sensitizes the Q lineage to perturbations that alter the Q.p division (see above). RNAi of all three *arf* genes, *arf-1.2*, *arf-3*, and *arf-6*, and mutations of *arf-1.2* and *arf-6* but not *arf-3*, produced extra-A/PVM phenotypes (Table 1). In contrast to the *arf* genes, RNAi or mutation of *arf*-related genes did not produce significant extra-A/PVM phenotypes (Table 1). Although *arf-3* is the best candidate for being the missing GTPase, its involvement in neuroblast asymmetric divisions that produce apoptotic cells remains uncertain (Singhvi *et al.* 2011). The RNAi phenotype of *arf-3* could result from off-target effects on *arf-1.2*, or the lack of a phenotype in the *arf-3* mutant could result from maternal rescue, since the mutation leads to larval arrest of homozygous mutants from heterozygous mothers.

We previously showed that *cnt-2* single and *cnt-2*; *arf-6* double mutants have a similar A/PVM phenotype, suggesting that *cnt-2* and *arf-6* function in the same genetic pathway (Singhvi *et al.* 2011). We also observed a suppression of the extra-A/PVM phenotype of a *cnt-2* mutant by an *arf-1.2* mutation, although this effect was explained by a failure of extra cells to express the A/PVM marker in double mutants

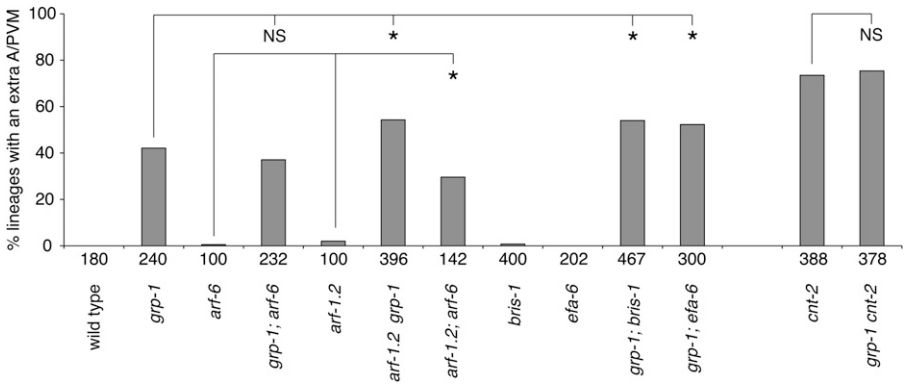

Figure 3 A/PVM phenotypes of *grp-1* and Arf pathway mutants. The *grp-1* extra-A/PVM phenotype was not enhanced by an *arf-6* mutation, but was enhanced by mutations in *arf-1.2* or the Arf GEF genes, *efa-6* and *bris-1*. The *cnt-2* Arf GAP mutant phenotype was not enhanced by *grp-1* or *arf-6* mutations. The *grp-1 cnt-2* double mutant also contained a *lon-1* mutation used in strain construction; control experiments showed no effect of *lon-1* on the penetrance of A/PVM phenotype of either *grp-1* or *cnt-2* mutants (data not shown). *bris-1(gk592726)* is a 5′ splice site hypomorphic mutant in the third intron of the predicted long *a* isoform, in the first intron of predicted *b* and *c* isoforms, and not affecting the predicted *d* isoform (TTGgtga > TTGatga). The number of lineages scored per genotype is shown under each bar. NS, not significant; $*P < 0.0001$.

rather than a true suppression of the extra cell production. Although the daughter cell size-symmetry defect of a *cnt-2* mutant was partially suppressed by the *arf-1.2* mutation, the number of extra cells and hence the apoptosis defect was not significantly altered. These results are consistent with *cnt-2* functioning together with *arf-1.2* and *arf-6* in the same cycle or cycles to regulate the Q.pp apoptotic fate and *arf-1.2* providing a separate function that regulates the differentiation of the extra cells (Singhvi *et al.* 2011).

To address whether *arf-1.2* and *arf-6* function in the same genetic pathway as *grp-1*, we examined the phenotypes of *arf*, *grp-1* double mutants and found that the *arf-1.2* but not the *arf-6* mutation enhanced the extra-A/PVM phenotype of the *grp-1* mutant (Figure 3). These data suggest either that GRP-1 could act in the same pathway as ARF-6 but in parallel to ARF-1.2 or that all three proteins could function together, with additional Arf GEFs able to compensate for *grp-1* loss and to activate ARF-1.2.

Loss of GRP-1 affects the sizes of the Q.p daughters: In wild-type animals, Q.p divides asymmetrically in size to generate a larger anterior cell that survives and a smaller posterior cell that dies (Figure 1B and Figure 5A). In *pig-1*, *arf-1.2*, and *cnt-2* mutants, a reduced cell-size asymmetry of the Q.p daughters was associated with the failure to specify PCD in the Q.pp cell (Cordes *et al.* 2006; Singhvi *et al.* 2011; Chien *et al.* 2012). The larger Q.pp in these mutants was often able to escape the death fate and adopt the mitotic fate of its sister, the anterior daughter cell of Q.p (Q.pa), to produce additional A/PVM and SDQ neurons. We observed that the Q.p division is more symmetric in the *grp-1* and *arf-6* mutants as well (Figure 4, B and C). Whereas *arf-6* did not enhance the cell-size defects of *grp-1* or *cnt-2* mutants, *arf-1.2* and *bris-1* were *grp-1* enhancers, consistent with the genetic interactions described for the A/PVM phenotype. Ou *et al.* (2010) showed that the Q.p daughter cell-size defect of *pig-1* mutants was not restricted to Q.p, but that the Q.a division was also more symmetric in the mutants. We observed similar Q.a division defects for *grp-1* and *cnt-2* (Figure S4). These results indicate that like *pig-1*, *grp-1* and *cnt-2* are general regulators of cell size asymmetries in the Q lineage.

The size asymmetry of the Q.p daughter cells correlates with extra cell production: We also scored the number of cells produced by the Q.p lineage using the *Pegl-17*::*mCherry* transgene (Figure 4D). This transgene expresses plasma membrane-bound and nuclear mCherry in the lineage and the mCherry markers persist after the A/PVM and SDQ neurons are born. To determine the number of cells produced by the Q.p lineage, we counted the number of mCherry-expressing cells in the positions of the Q.p descendants. In the *grp-1* mutant, 57% of Q.p lineages produced one or two extra neurons (Figure 4D), which is higher than the frequency of lineages that produce extra-A/PVM neurons. This discrepancy may be due to the inability of some of the extra cells to choose a fate, as has been suggested for the "undead" cells produced in cell death mutants (Ellis and Horvitz 1986; Guenther and Garriga 1996; Cordes *et al.* 2006). The genetic interactions seen when scoring the sizes of daughter cells and the extra-Q.p-derived neurons were similar: the *arf-6* mutation did not significantly alter the frequency of extra cells produced by *grp-1* or *cnt-2* mutants, the *arf-1.2 arf-6* double mutant had an increased numbers of extra cells compared to the single mutants, and the *arf-1.2* mutation enhanced the *grp-1* phenotype (Figure 4D).

Since these different mutant combinations displayed a range of cell size and extra-cell phenotypes, we tested whether there was a relationship between the two datasets. We indeed observed that decreased size asymmetry of the Q.p daughters and the production of extra-Q.p progeny are strongly correlated (Figure S5).

GRP-1 and ARF-6 function autonomously in the Q lineage

To determine the site of *grp-1* function, we first analyzed animals that were functionally mosaic for *grp-1*. Since the A/PVM phenotype is incompletely penetrant, we screened

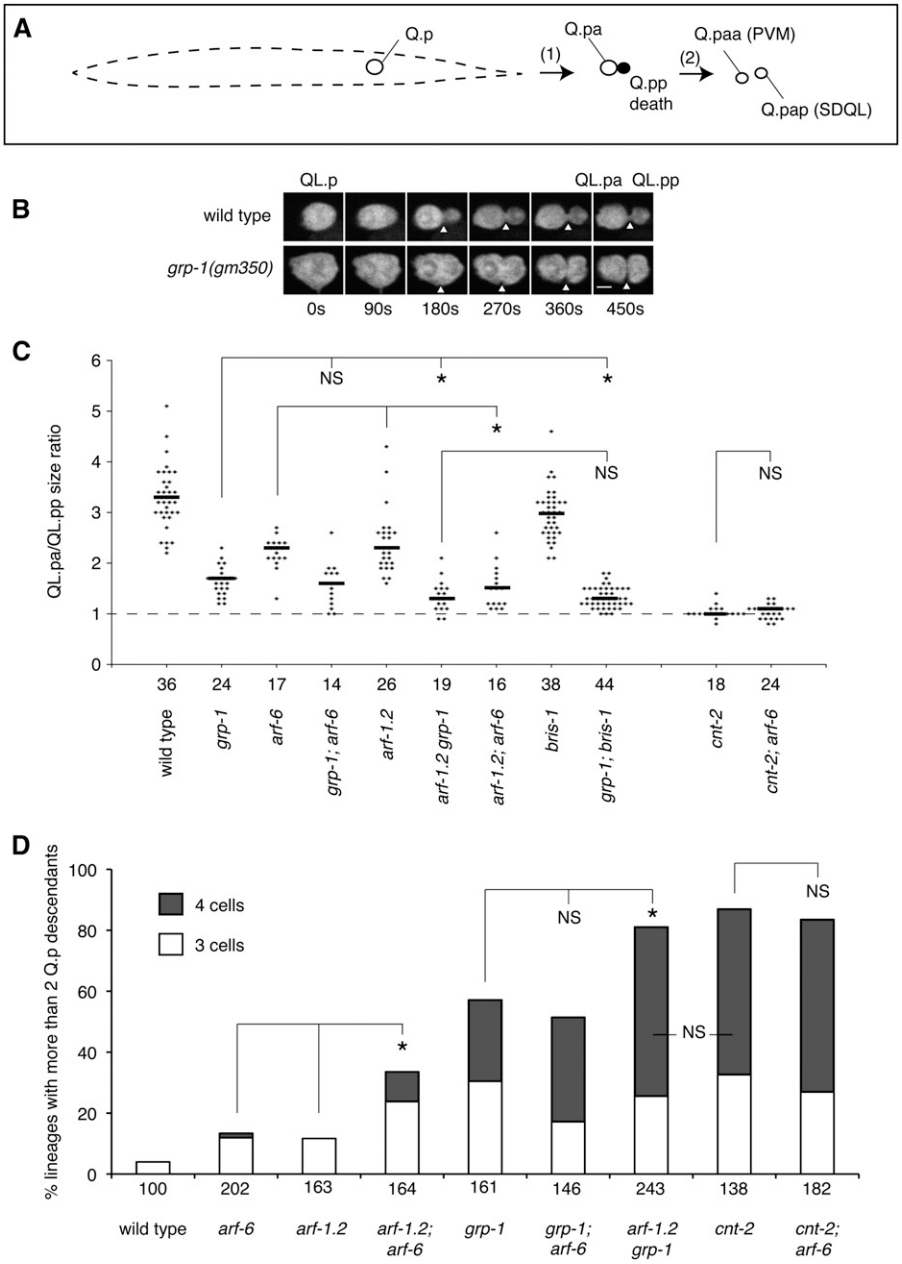

Figure 4 Analysis of QL.p cell division and progeny in *grp-1* and *arf* mutants. (A) Schematic representation of the wild-type QL.p neuroblast development (dashed outline represents an L1 larva). QL.p divides asymmetrically (1) and gives rise to a larger Q.pa and a smaller Q.pp, which is fated to die. After the division of the surviving Q.pa (2), the two cells produced differentiate as the PVM (Q.paa) and the SDQL (Q.pap). (B) Fluorescence photomicrographs from time-lapse recordings of wild-type and *grp-1(gm350)* QL.p divisions. Animals contained the *Pegl-17*::*gfp* transgene *aylS9*. Arrowheads indicate the position of the cleavage furrow. Numbers at the bottom of each frame represent the time in seconds. The Q.p cell exhibits a range of sizes, and the one from the *grp-1* mutant shown here is at the larger end of the size range. Although this cell is larger than the wild-type Q.p cell, the size range of wild-type and mutant Q.p cells was similar. Bar, 2 μm. (C) Cell-size ratios of the QL.p daughters. The cell sizes of the Q.p daughters were determined by measuring the area of cells expressing the *rdvIs1*[*Pegl-17*::*myristoylated mCherry*] transgene. Each dot corresponds to the size ratio of one pair of Q.p daughters, and the horizontal bars indicate the median of the ratio distribution. The dashed horizontal line indicates a 1:1 ratio, where the Q.p daughter cells are of equivalent size. (D) Total number of surviving Q.p descendants. The number of daughter pairs (C) and lineages (D) scored per genotype is shown under each bar. NS, not significant; $^*P < 0.0001$.

for mosaic animals with extra AVMs or PVMs and determined which cells had lost the rescuing array. All of the mutant animals had lost the array in the lineage that produced the extra AVM or PVM (Figure S6). The most informative loss was in AB.plapapa, four divisions before the production of the Q.p. We conclude from the mosaic experiment that *grp-1* functions in the progeny of AB.plapapa.

To ask whether *grp-1* acts in the Q lineage, we generated transgenes driving *grp-1*::*gfp* expression from the *mab-5* promoter. The gene *mab-5* encodes a homeobox transcription factor that is expressed in many posterior cells on both sides of the animal (Cowing and Kenyon 1992). The one exception to this bilateral expression in young L1 larvae is the Q lineage: *mab-5* is expressed in the left Q.p lineage, which produces PVM, but not in the right, which produces AVM (Figure 5A) (Salser and Kenyon 1992). We reasoned that if *grp-1* functions autonomously in the Q lineage, then the *Pmab-5*::*grp-1*::*gfp* transgene would rescue the extra-PVM phenotype, but not the extra-AVM phenotype. If *grp-1* functions nonautonomously then the transgene might rescue both the AVM and PVM phenotypes or neither phenotype. We used this approach to show that *pig-1*, *cnt-2*, and *arf-1.2* function cell autonomously in the Q lineage (Cordes *et al.* 2006; Singhvi *et al.* 2011). In two of the three transgenic lines that we tested, we found that the *Pmab-5*::*grp-1*::*gfp* construct rescued the PVM but not the AVM phenotype (Figure 5B and data not shown). We performed a similar experiment to examine *arf-6* autonomy. Although *arf-6* mutants

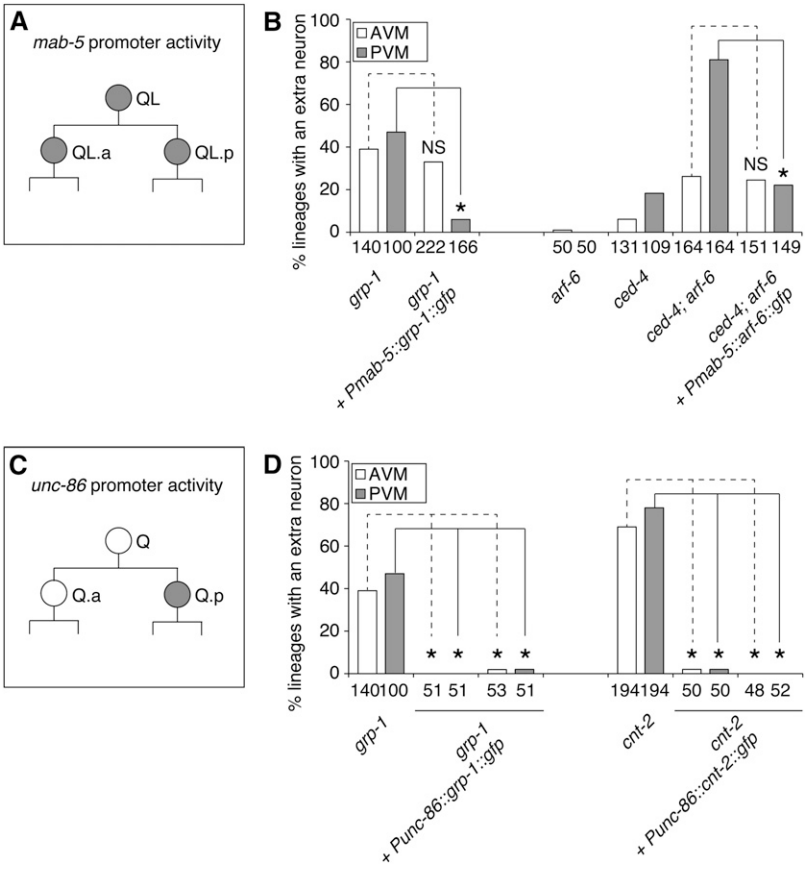

Figure 5 GRP-1 functions autonomously. (A and C) Schematic diagrams of the Q neuroblast lineage indicating the specific cells where the promoters are expressed. (A) The *mab-5* promoter is active (shaded cells) in the left Q lineage. (B) Expressing *grp-1* or *arf-6* from the *mab-5* promoter rescued the QL but not the QR lineage defects of the *grp-1(gm350)* and *ced-4*; *arf-6* mutants, respectively. (C) The *unc-86* promoter is active (shaded cell) in the left and right Q.p cells before they divide. (D) Expressing *grp-1* or *cnt-2* from the *unc-86* promoter rescued the extra-A/PVM defects of the *grp-1(gm350)* and *cnt-2(gm377)* mutants, respectively. For each rescue experiment in D, two independent transgenic lines are shown. The number of lineages scored per genotype and side is shown under each bar. NS, not significant; $*P < 0.0001$ for rescue of the A/PVM defects.

do not produce extra A/PVMs, they can display an extra-A/PVM phenotype in sensitized genetic backgrounds where the caspase activation cascade is impaired, such as the *ced-4*/APAF mutant (Singhvi *et al.* 2011). We observed that a *Pmab-5*::*arf-6*::*GFP* integrated transgene suppressed the PVM, but not the AVM defects of *ced-4*; *arf-6* double mutants (Figure 5B). These results suggest that, like *cnt-2*, *arf-1.2* and *pig-1*, *grp-1* and *arf-6* act autonomously in the Q lineage.

GRP-1 and CNT-2 function autonomously in Q.p: Although our results indicate that *grp-1* and *cnt-2* function in the Q lineage to regulate Q.p asymmetric division, they are compatible with a function in the Q neuroblast, the Q.p cell itself, its sister Q.a, or any combination of these cells. To pinpoint where *grp-1* and *cnt-2* function, we drove the expression of functional GRP-1::GFP and CNT-2::GFP fusions in Q.p using the *unc-86* promoter. The gene *unc-86* encodes a POU-domain transcription factor required for cell-fate specification in many *C. elegans* neuroblast lineages (Finney *et al.* 1988). In the Q neuroblast lineage, the *unc-86* promoter is active in Q.p before its division (Figure 5C) (Baumeister *et al.* 1996). We observed that expressing GRP-1::GFP and CNT-2::GFP in Q.p, rescued, respectively, the *grp-1* and *cnt-2* A/PVM mutant phenotypes (Figure 5D).

The ability of the *unc-86* promoter-driven expression of *grp-1* and *cnt-2* to rescue the A/PVM phenotypes of the mutants suggests that GRP-1 and CNT-2 act in Q.p to regulate the asymmetry of its division. Both proteins are normally expressed in Q.p and its daughter cells (data not shown). This expression raises the question of whether these proteins act solely in Q.p to regulate the asymmetry of the division, which contributes to Q.pp apoptosis, or whether they act both in Q.p to regulate the asymmetry of the division and in Q.pp to promote apoptosis. We currently do not know whether GRP-1 and CNT-2 function in Q.pp to promote its apoptotic fate.

Structure/function analysis of GRP-1

We used deletion and mutational analysis to better characterize the three GRP-1 domains. All of these experiments were conducted by expressing a *grp-1* cDNA or cDNA fragments fused to GFP from the *dpy-30* promoter, which drives widespread expression, in *zdIs5*; *grp-1(gm350)* mutants. This broad expression allowed us to observe GFP localization in embryonic cells and to address whether the constructs rescued the A/PVM phenotype in larvae. In these experiments, GFP was fused to the C terminus of GRP-1, and like GFP::GRP-1 (Figure 2), GRP-1::GFP localized to nuclei and rescued the *grp-1* A/PVM phenotype (Figure 6, A, B, B′, and G).

In light of the importance of the CC and PH domains in regulating the activity of vertebrate cytohesins, we performed experiments to determine whether these domains

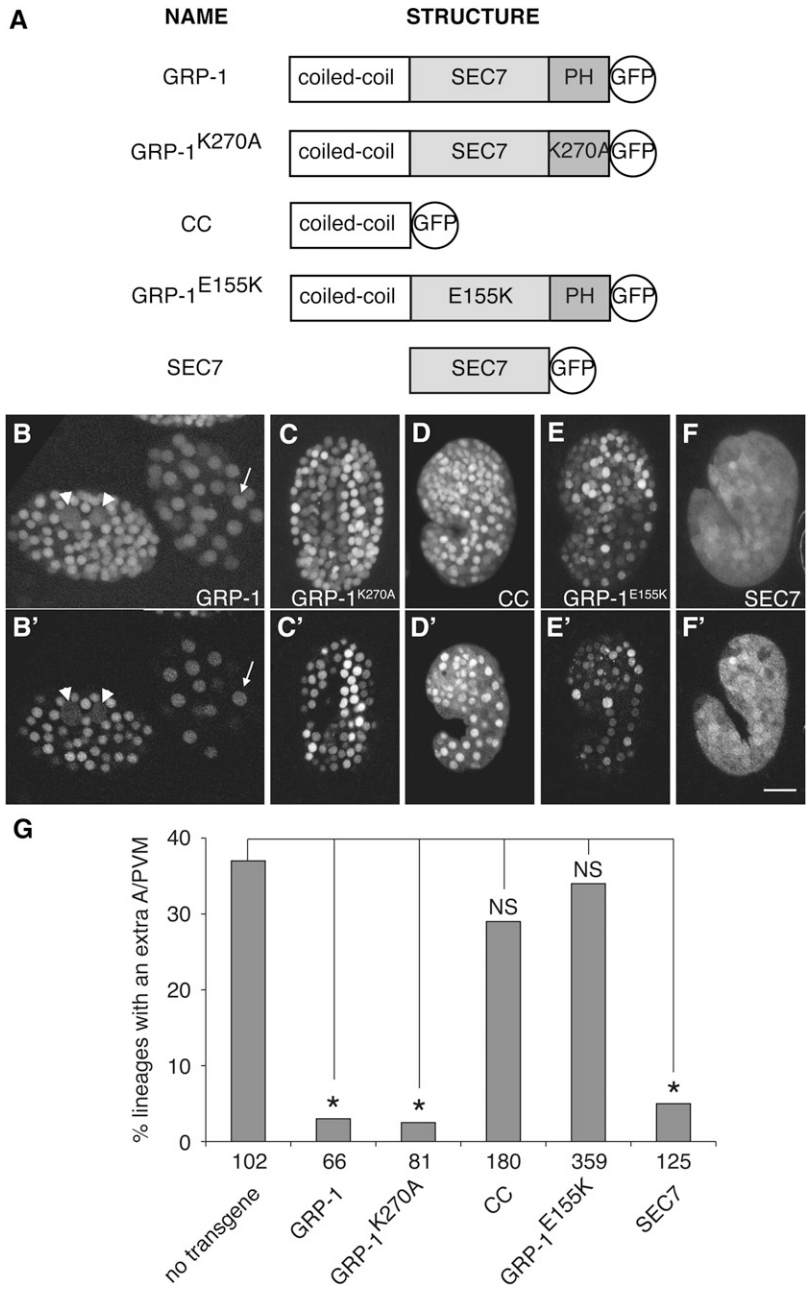

Figure 6 GRP-1 structure–function analysis. (A) Diagrams of the GRP-1–GFP proteins used. All constructs were expressed from the *dpy-30* promoter, which drives broad expression. (B–F) Confocal projections and (B′–F′) individual slices from the same confocals series. *zdIs5* [*mec-4*::*gfp*]; *grp-1(gm350)* embryos expressing (B and B′) GRP-1::GFP, (C and C′) the GRP-1^{K270A} PH domain mutant, (D and D′) the GRP-1 coiled-coil (CC) domain, (E and E′) the GRP-1^{E155K} GEF-dead mutant, and (F and F′) the SEC7 domain. Bar, 10 μm. (G) Ability of the different transgenes to rescue the A/PVM phenotype of *grp-1(gm350)* mutants. The number of lineages scored per genotype is shown under each bar. NS, not significant; $^*P < 0.001$ in comparison to nontrangenic *grp-1* mutants.

were necessary or sufficient for GRP-1 activity. First, we mutated a critical lysine residue in the GRP-1 PH domain that vertebrate cytohesins require to bind PI(4,5)P_2 and PI(3,4,5)P_3 (Klarlund *et al.* 2000; Cronin *et al.* 2004). The GRP-1^{K270A} mutant did not affect GRP-1 rescuing activity nor did it affect the localization of GRP-1 to nuclei (Figure 6, A, C, C′, and G). Second, we determined whether the GRP-1 PH domain could function as a dominant negative, as has been described previously for vertebrate cytohesins (Kolanus *et al.* 1996; Várnai *et al.* 2005). We targeted the GRP-1 PH domain to either the nucleus (NLS-PH) or cell cortex (MYR-PH), but did not observe an extra-A/PVM phenotype in wild-type animals or *ced-3(n717)* mutants sensitized to the loss of GRP-1 activity (data not shown). Third, although predominantly localized in nuclei like the full-length GRP-1, a deletion mutant containing only the GRP-1 CC domain neither rescued the *grp-1* mutant (Figure 6, A, D, D′, and G) nor produced extra neurons in a wild-type *grp-1* background (data not shown). Finally, the hypomorphic *grp-1(gk402275)* mutant, which is predicted to produce a GRP-1 protein with a PH domain truncation, displayed only a weak extra-A/PVM defect (Figure 1D).

Experiments conducted in cultured cell lines indicate that the Arf GEF activity of the SEC7 domain is required for cytohesin function. The Arf GEF activity of vertebrate cytohesins is disrupted by mutation of a conserved glutamate codon to lysine in the SEC7 domain (Cherfils *et al.* 1998; Mossessova *et al.* 1998). We found that GRP-1 with the

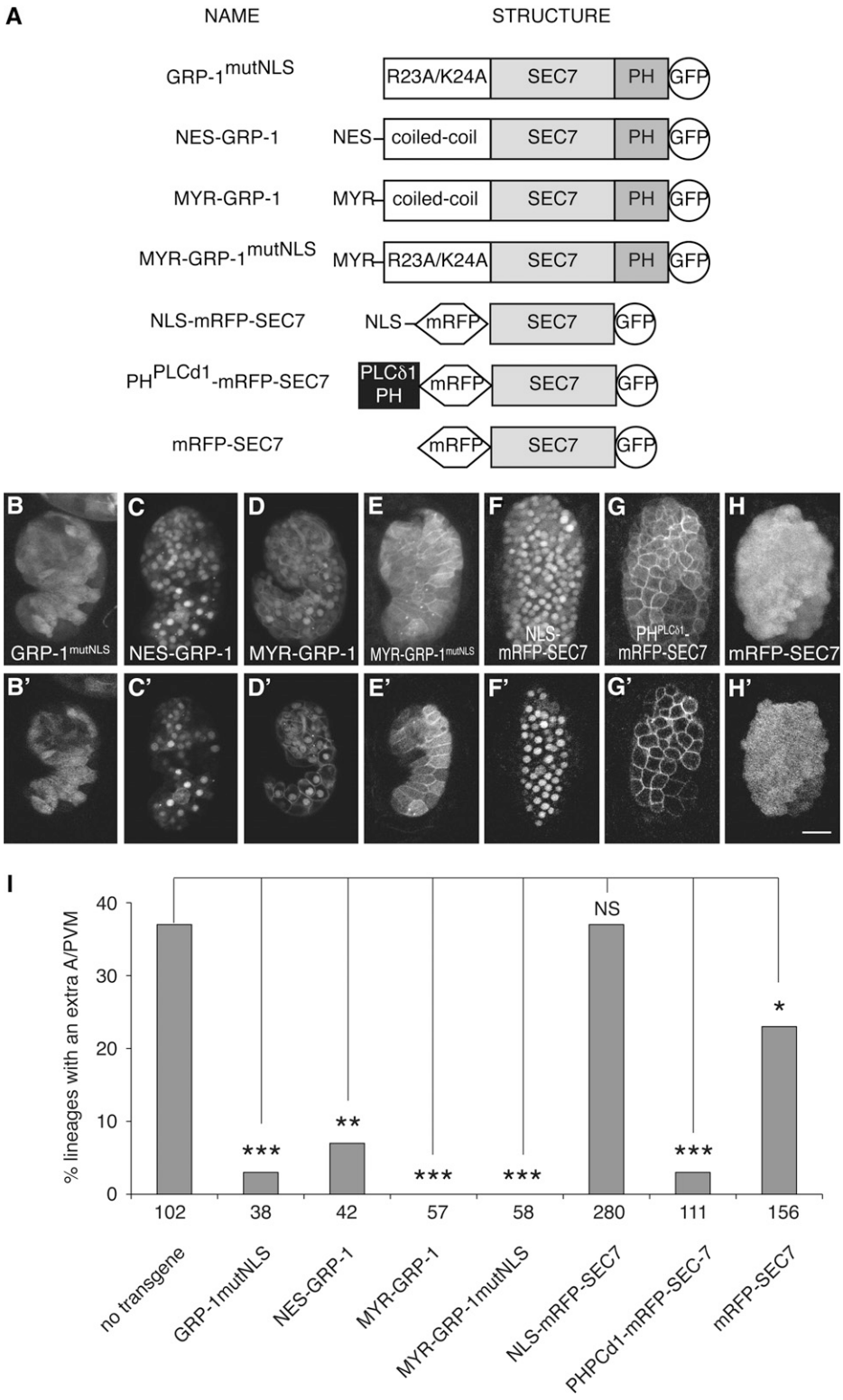

Figure 7 Subcellular localization and function of GRP-1::GFP proteins. (A) Diagram of mutant and modified GRP-1–GFP proteins used. All constructs were expressed from the *dpy-30* promoter, which drives broad expression. (B–H) Confocal projections, and (B′–H′) individual slices from the related confocal series. *zdls5* [*mec-4*::*gfp*]; *grp-1 (gm350)* embryos expressing (B and B′) GRP-1 carrying a mutation in the NLS found in the CC domain, (C and C′) GRP-1 containing an NES, (D and D′) myristoylated GRP-1, (E and E′) myristoylated GRP-1 containing a mutated NLS, (F and F′) an mRFP::SEC7:: GFP protein containing an NLS, (G and G′) an mRFP::SEC7:: GFP protein containing a PLCδ1 PH domain, and (H and H′) an mRFP::SEC7:: GFP protein. The signal from the mRFP::SEC7::GFP trangenes, made with constructs injected at low concentration, was fainter than the other transgenes, and contrast adjustment was used to reveal subcellular localization of the fusion proteins. Bar, 10 μm. (I) Ability of the different transgenes to rescue the A/PVM phenotype of *grp-1(gm350)* mutants. The number of lineages scored per genotype is shown under each bar. NS, not significant; $*P < 0.02$, $**P < 0.0005$, $***P < 0.0001$ in comparison to nontransgenic *grp-1* mutants.

analogous E155K mutation failed to rescue the extra-A/PVM phenotype of the *grp-1(gm350)* mutant but localized similarly to wild-type GRP-1 (GRP-1^{E155K}; Figure 6, A, E, E′, and G). Expressing a mutant containing only the GRP-1 SEC7 domain rescued the extra-A/PVM phenotype (Figure 6, A and G), and this fusion localized broadly throughout both the cytoplasm and nucleus (SEC7; Figure 6, F and F′). Taken together, these findings suggest that the CC and PH domains are not essential and that Arf GEF activity is necessary and sufficient for GRP-1-dependent regulation of asymmetric neuroblast divisions, at least under conditions where the fusions were expressed from multicopy transgenes.

Nuclear localization signals in GRP-1: GFP::GRP-1 localization to the nucleus (Figure 2) compelled us to ask which GRP-1 domains were necessary for GRP-1 function and nuclear localization. To identify regions necessary for GRP-1 subcellular localization and function, we examined deletion mutants lacking certain GRP-1 domains. Subcellular localization of two fusions proteins suggested that the GRP-1 CC domain contained a nuclear-localization sequence (NLS): a fusion containing only the CC domain was strongly enriched in nuclei, while a fusion containing only the SEC7 domain was not (Figure 6, D, D′, F, and F′). These data led us to identify a putative NLS (PKVRKRK) in the CC domain using the PPSORT II algorithm (Cherfils *et al.* 1998; Mossessova *et al.* 1998; Nakai and Horton 1999). To determine whether this sequence functions as a NLS, we mutated it to PKVAARK in a full-length GRP-1 fusion construct (Figure 7A, GRP-1^{mutNLS}), designing these mutations so that they would not interfere with the repeated structure of the coiled-coil domain. We found that the resulting GRP-1^{mutNLS} fusion was evenly distributed between the nucleus and cytoplasm, suggesting that this sequence contributes to the nuclear localization of GRP-1 (Figure 7, B and B′). The continued presence of GRP-1^{mutNLS} in nuclei may be due to an additional cryptic NLS in the SEC7 domain, as the SEC7 fusion and a similar construct with an additional mRFP moiety (mRFP-SEC7) were still present in nuclei (Figure 7, F and F′).

GRP-1 may function at the plasma membrane

The novel nuclear localization of GRP-1 led us to ask whether GRP-1 functioned in nuclei to regulate asymmetric neuroblast divisions. The first series of experiments we performed was designed to prevent GRP-1's nuclear localization. We mutated the GRP-1 NLS (GRP-1^{mutNLS}), added a nuclear export signal (NES-GRP-1), targeted the protein to the plasma membrane using a myristoylation signal (MYR-GRP-1), and made a fusion with both a mutant NLS and a myristoylation signal (MYR-GRP-1^{mutNLS}) (Figure 7, A–E′ and I). None of these modifications eliminated GRP-1 entirely from nuclei, and all of these constructs rescued the *grp-1(gm350)* mutant phenotype, providing little insight as to whether GRP-1 functions in nuclei. When placed in a wild-type background, the GRP-1^{mutNLS} and the NES-GRP-1 did not perturb the asymmetric divisions of either the Q.p or the Q.a neuroblasts, indicating that delocalizing GRP-1 in interphase does not generate defects in the Q lineage (data not shown).

Because the SEC7 domain alone was partially active in the rescue assays (Figure 6G), we next asked whether targeting the SEC7 domain to different subcellular compartments would affect the ability of the SEC7 domain to rescue the mutant A/PVM phenotypes. We created three constructs, one targeted to the nucleus (NLS-mRFP-SEC7), one to the cell cortex (PH^{PLCdelta1}-mRFP-SEC7), and one untargeted control (mRFP-SEC7) (Figure 7A). To prevent passive diffusion into the nucleus, all three constructs contained both mRFP and GFP (GFP is not indicated in construct name) to increase the size of the fusion protein, and we reduced the concentration of the injected DNA to minimize effects caused by excess expression (Table S1). As expected, the NLS-mRFP-SEC7 fusion was found concentrated in nuclei, and the PH^{PLCdelta1}-mRFP-SEC7 to the plasma membrane (Figure 7, F–G′). The untargeted mRFP-SEC7 fusion was present uniformly throughout the cytoplasm and nucleus, even though it should be too large to passively diffuse into nuclei (Figure 7, H and H′). This latter result suggested that an additional cryptic NLS might exist in the SEC7 domain. When we examined these constructs in our phenotypic rescue assay, we found that the NLS-mRFP-SEC7 fusion did not rescue *grp-1*, that the mRFP-SEC7 fusion rescued partially, and that the PH^{PLCdelta1}-mRFP-SEC7 fusion rescued completely (Figure 7I). There is a discrepancy between the partial rescue by the mRFP-SEC7 fusion and the complete rescue observed with the SEC7 fusion (Figure 5G). This could be explained by the addition of the mRFP at the N terminus; however, this possibility seems unlikely since this tag did not perturb the activity of the rescuing PH^{PLCdelta1}-mRFP-SEC7 fusion. The other possibility is that the SEC7 domain cannot efficiently rescue the *grp-1* phenotype at low expression levels, suggesting auxiliary roles played by the CC and PH domain in the full-length GRP-1 protein. These observations strongly suggest that GRP-1 functions at the cell periphery to regulate asymmetric neuroblast divisions.

Targeting Arf GEF activity to the cell periphery is sufficient to restore grp-1 function

Although the experiments described above suggest that the GRP-1's Arf GEF activity is required at the cell surface, it is possible that, due to the cryptic NLS sequence in the SEC7 domain, the PH^{PLCdelta1}-mRFP-SEC7 fusion is present in the nucleus at undetectable levels. We thus tried to restore Arf GEF activity in Q.p using an alternative GEF, EFA-6, which exclusively localized to the plasma membrane. The EFA-6 protein contains a SEC7 domain and a PH domain like GRP-1, but its structure differs in the N- and C-terminal domains. EFA-6 has been shown to regulate cortical microtubules dynamics in the *C. elegans* embryo, an activity dependent on a conserved short N-terminal motif (microtubule regulating region, MTR) but independent of the SEC7 domain (O'Rourke *et al.* 2010).

GFP fusions to a functional EFA-6, a GEF dead mutant (EFA-6^{E447K}), and a MTR-deleted mutant (EFA-6$^{\Delta MTR}$) were expressed in the QL lineage using the *mab-5* promoter (Figure 8A). We confirmed that EFA-6 localized at the cell periphery in the QL lineage and other cells where the *mab-5* promoter is active (Figure 8, B–D′). The analysis of the A/PVM phenotype of *grp-1* mutants carrying these transgenes revealed that full-length EFA-6 and EFA-6$^{\Delta MTR}$ rescued the *grp-1* mutant, but the SEC7 EFA-6^{E447K} did not (Figure 8E). These results support the hypothesis that GRP-1 GEF activity is required at the plasma membrane and not in the nucleus.

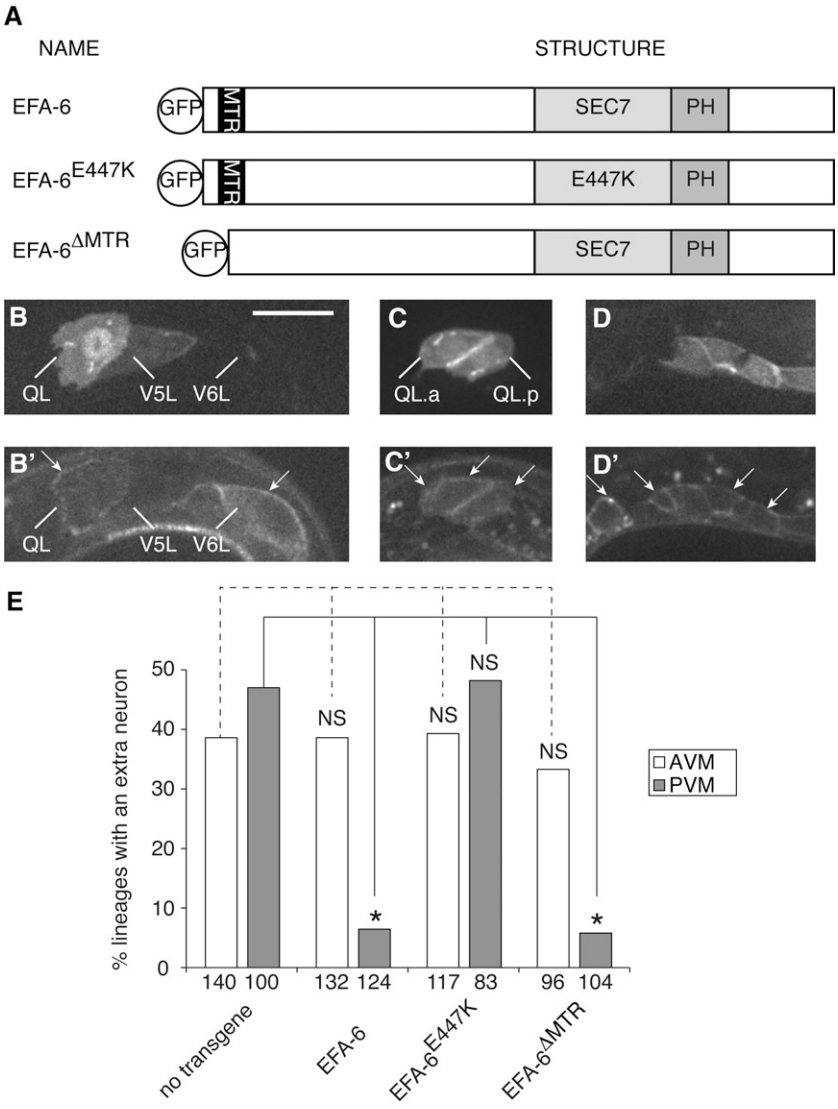

Figure 8 The Arf GEF EFA-6 can replace GRP-1's requirement in a SEC7-dependent manner. (A) Diagrams of the EFA-6–GFP proteins used to rescue the *grp-1* A/PVM phenotype. The *mab-5* promoter drove expression in the left Q lineage. MTR, microtubule-regulating motif; PH, pleckstrin-homology domain. (B–D′) Confocal micrographs showing the localization of GFP::EFA-6 in *grp-1 rdvIs1* larvae. (B–D) Labeled plasma membranes and nuclei of cells expressing the *rdvIs1* mCherry markers. (B′–D′) Labeled plasma membranes (arrows) of cells expressing the *Pmab-5*::*gfp*::*efa-6* transgene. The GFP::EFA-6 cells indicated by arrows are QL and V5L (B′), QL.a and QL.p (C′), and posterior P lineage-derived cells (D′). Bar, 10 μm. (E) Ability of different *Pmab-5*::*gfp*::*efa-6* transgenes to rescue the extra-PVM phenotype of *grp-1(gm350)* mutants. The number of lineages scored per genotype and per side is shown under each bar. NS, not significant; $*P < 0.0001$.

Endogenous GRP-1 protein localizes to midbodies

We observed that GRP-1–GFP fusions accumulate in interphase nuclei, but our rescue experiments indicate that the ARF GEF functions at the plasma membrane. We reasoned that GRP-1 may accumulate at the membrane at the time of its cytoplasmic release by the nuclear membrane breakdown during mitosis (Figure 6, B and B′). However, the cytoplasmic GFP signal was too bright to allow us to detect a specific accumulation of GRP-1 at the surface, and lowering the expression of GRP-1::GFP fusions by the use of rescuing low-copy number transgenes (Figure 5D) rendered the GFP undetectable in Q.p cells (data not shown). To examine the endogenous localization of GRP-1 during mitosis, we raised antibodies against a GRP-1 peptide and immunolabeled *C. elegans* embryos.

We were able to detect punctate, ring-like signals between cells in wild-type embryos (Figure 9, A and B). These punctae were not detected in the *grp-1* mutants, suggesting that the immunolabeling was specific for the GRP-1 protein (Figure 9C). The punctae appeared similar to the cytokinetic furrow remnants, or midbodies. The GRP-1 punctate signal colocalized with both NMY-2/nonmuscle myosin II heavy chain and ZEN-4/MKLP/Pavarotti, two markers of the midbody (Figure 9, D and E). Localization of endogenous GRP-1 at midbodies could have two explanations. First, GRP-1 could be recruited to the midbody after cytokinesis (Figure 9F). Second, GRP-1 could be recruited to the cleavage furrow before or during its ingression and accumulate at the midbody upon completion of cytokinesis (Figure 9G). In this latter model, we would only be able to detect GRP-1 with our antibodies when the protein is concentrated at midbodies. We were unable to detect endogenous GRP-1 in cell nuclei by immunolabeling. Together, these data support a model where the GRP-1 Arf GEF functions at the cell periphery in mitotic cells.

Discussion

We show that GRP-1, the *C. elegans* homolog of vertebrate cytohesin Arf GEFs, regulates the asymmetry of certain neuroblast divisions and their ability to generate a daughter cell that adopts the apoptotic fate. To our knowledge, this is the first

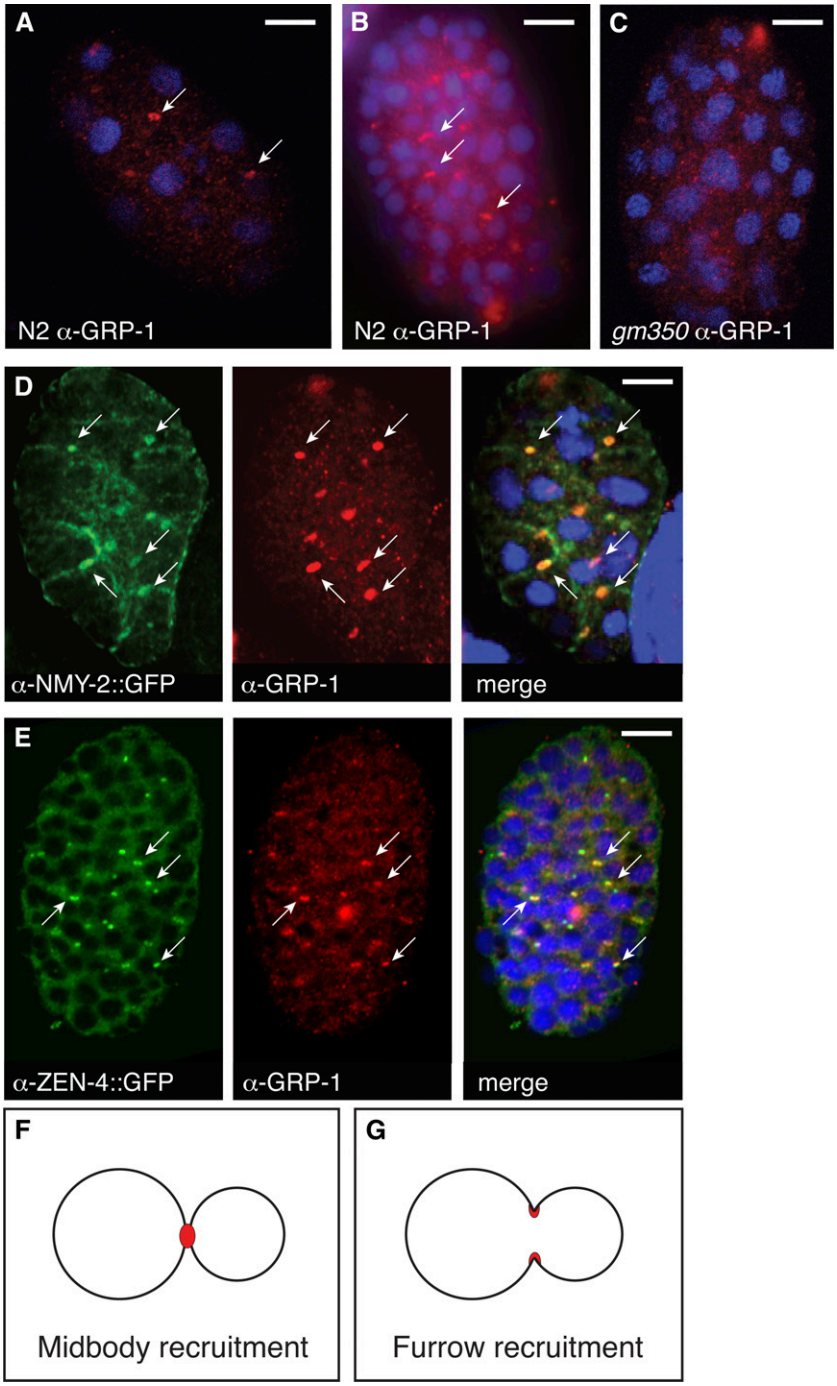

Figure 9 Immunolabeling of endogenous GRP-1 protein at midbodies. DAPI (blue) was used to counterstain nuclei in all merge photomicrographs. (A and B) Immunofluorescence staining of GRP-1 (red) in an early (A) and a late (B) stage wild-type (N2) embryo. GRP-1 localized to ring-like structures between cells (arrows). (C) Absence of GRP-1 staining in a *grp-1(gm350)* mutant embryo. (D and E) Immunofluorescence staining of wild-type embryos that expressed the myosin II fusion NMY-2::GFP (D, green, left), the ZEN-4::GFP fusion (E, green, left), and endogenous GRP-1 (D and E, red, center). The merged panels (right) show colocalization of GRP-1 at midbodies marked with NMY-2::GFP and ZEN-4::GFP (arrows). Bars, 10 μm. (F and G) Models for the timing of GRP-1 recruitment to the cell surface. (F) GRP-1 is recruited to the midbody at the end of cytokinesis. (G) GRP-1 is recruited to the furrow during cytokinesis and accumulates at the midbody.

report of a role for a cytohesin in the asymmetry of cell divisions. We demonstrate that the ARF GEF activity of GRP-1 at the plasma membrane is both necessary and sufficient for GRP-1 to regulate asymmetric neuroblast divisions and identify ARF-6 and the Arf GAP CNT-2 as potential components of the same Arf cycle that regulates these divisions.

Daughter cell-size asymmetry and cell death specification

By analyzing the sizes of Q.p daughter cells in various mutants, we observed that an increase in the cell size of the posterior daughter correlated with the loss of its apoptotic fate. Although there is no direct evidence of a causal relationship between a small cell size and cell death in *C. elegans*, two additional studies support a model where increased cell size interferes with the ability of a cell to adopt the apoptotic fate. First, the asymmetric division of the NSM precursor to generate the NSM neuron and its sister cell, which is fated to die, is more symmetric in *dnj-11* mutants (Hatzold and Conradt 2008). Following the NSM precursor division in *dnj-11* mutants, the authors observed a range of altered daughter cell sizes and noted a correlation between

a larger daughter cell size and the inability of the cell to adopt an apoptotic fate. Second, Ou *et al.* (2010) showed that the Q.p neuroblast sister, Q.a, produces a smaller anterior cell by a mechanism dependent on anterior myosin II accumulation. CALI experiments that inactivated the asymmetrically distributed NMY-2::GFP in Q.a also resulted in a more symmetric division and differentiation of Q.aa, the cell normally fated to die.

Recent studies in HeLa cells dividing on patterned substrates showed that a failure to divide symmetrically was occasionally associated with the death of the smaller cell (Kiyomitsu and Cheeseman 2013). One possibility is that the activation of the caspase pathway and a reduction in cell size both can contribute to the induction of cell death. How the cell size might tip the balance toward cell death instead of survival remains to be determined.

C. elegans Arf GTPases can compensate for each other's inactivation

We observed that *C. elegans* can survive in the absence of both class I and III Arfs: *arf-1.2*; *arf-6* double mutants are sick but viable. The *C. elegans* class II Arf, ARF-3, is sufficient for viability in the absence of class I and III Arfs. This observation indicates that ARF-3 or the Arls can perform all Arf-dependent essential functions. This view is supported by studies showing that specific members of all three Arf classes can support recruitment of coatomer to Golgi membranes *in vitro* and that knocking down the functions of more than one Arf is necessary to disrupt specific membrane trafficking events (Liang and Kornfeld 1997; Volpicelli-Daley *et al.* 2005). A more recent study showed that the *in vitro* production of COPI vesicles can be promoted by several Arfs including Arf3, but that in the presence of other Arfs, Arf3 was excluded from the vesicles, highlighting the promiscuity of Arf function when certain Arfs are lost (Popoff *et al.* 2011). In summary, our studies of the *arf* mutants suggest that *in vivo* the Arfs can provide overlapping functions in the regulation of essential cellular activities such as secretion and endocytosis.

Arf pathways regulate asymmetric neuroblast divisions: Our data indicate that ARF-6, GRP-1, and CNT-2 could act in the same Arf cycle to regulate Q.p asymmetric division. Furthermore, other Arfs, such as ARF-1.2 and ARF-3, and GEFs, such as EFA-6 and BRIS-1, may act in the same Arf cycle or define one or more additional CNT-2-dependent cycles. How could class I and III Arfs provide overlapping functions for the Q.p division? ARF-1.2 and ARF-6 might function in the same process. For example, all three Arf classes have been shown to activate PLD and PI5K, suggesting that GRP-1 could regulate asymmetric neuroblast divisions by controlling the production of a lipid intracellular signal (Godi *et al.* 1999; Honda *et al.* 1999; Jones *et al.* 2000). Alternatively, ARF-1.2 and ARF-6 could have different outputs; for example, they could regulate separate trafficking steps. One possibility is that GRP-1 regulates protein trafficking in the endocytic pathway, as there is evidence that Arf1 and Arf6 can regulate different aspects of trafficking to or from endosomes (Randazzo *et al.* 2000; Donaldson 2003; Nie *et al.* 2003).

Cytohesins can act as exchange factors for both Arf1 and Arf6 *in vitro* (Casanova 2007). Arf6-GTP and to a lesser extent Arf1-GTP can also activate cytohesins, relieving an autoinhibition mediated by interactions between the Sec7 and PH domains and converting them from their inactive cytoplasmic form to their active membrane-bound form (Cohen *et al.* 2007; DiNitto *et al.* 2007; Hofmann *et al.* 2007; Li *et al.* 2007). The findings that Arfs can function as cytohesin activators and effectors led Stalder *et al.* (2011) to propose that Arfs and the cytohesin ARNO act in a positive feedback loop *in vitro*. In *C. elegans*, genetic interactions are consistent with ARF-6 acting as a GRP-1 activator, effector, or both.

GRP-1 functions at the cell surface despite a predominantly nuclear localization

The localization of GFP-tagged GRP-1 to nuclei was unexpected. The ability of the $PH^{PLCdelta1}$-tagged SEC7 domain but not the NLS-tagged SEC7 domain to rescue the extra-A/PVM phenotype indicates that membrane-associated and not nuclear GRP-1 functions to regulate asymmetric neuroblast divisions. The rescue of *grp-1* defects by the Arf GEF EFA-6 and the human cytohesin CYTH2, which localized to the cell periphery and not the nucleus, and the detection of endogenous GRP-1 in midbodies, further support this model.

While casual inspection of *grp-1* mutant nuclei and nucleoli did not reveal any obvious phenotypes, it remains possible that GRP-1 has nuclear functions unrelated to its role in asymmetric divisions.

An alternative explanation for nuclear localization is to sequester GRP-1, either to remove excess GRP-1 from its site of function at the plasma membrane or to time its access to the plasma membrane at nuclear breakdown during mitosis. This model predicts that disruption of this nuclear sequestration should generate a phenotype. When we expressed some of the mutant GRP-1 proteins with an increased cytoplasmic localization in a wild-type background, however, we observed apparently normal Q.a and Q.p divisions (data not shown), suggesting that the cytoplasmic GRP-1 localization is not detrimental for the development of the Q lineage.

Mechanism of asymmetry

Our results suggest that Arf-dependent trafficking and the PIG-1 kinase function in a general mechanism that establish daughter cell-size asymmetry in *C. elegans*. The genes *pig-1*, *grp-1*, *arf-1.2*, and *arf-3* also regulate cell shedding, a process that occurs in caspase-deficient mutants and results in the death of specific cells generated early in embryogenesis (Denning *et al.* 2012). In addition, *pig-1* functions with the LKB-1/STRAD/MO25 polarity complex in both cell shedding and the asymmetric cell divisions described in this article (Chien *et al.* 2012; Denning *et al.* 2012). Denning *et al.* (2012) observed that mutations in *pig-1*, *grp-1*, *arf-1.2*, or

arf-3 suppressed the shedding and death caused by loss of caspase activity and proposed that these genes negatively regulate adhesion of the shed cells to their neighbors. In their model, mutations in these genes increased adhesion, interfering with shedding and allowing the cells to survive. Our analysis of *grp-1* and the findings of other studies demonstrate that mutations in the genes *pig-1*, *grp-1*, *arf-1.2*, or *arf-3* can cause the transformation of cells that normally die into their sister cells (Cordes *et al.* 2006; Ou *et al.* 2010; Singhvi *et al.* 2011; Chien *et al.* 2012). We propose that the cell shedding defects of *pig-1*, *grp-1*, *arf-1.2*, and *arf-3* mutants observed by Denning *et al.* (2012) result from defects in the asymmetric divisions that produce the shed cells. In this model, the daughter cell that would normally be shed in the caspase-deficient mutant instead adopts the fate of its sister in the *pig-1*, *grp-1*, *arf-1.2*, or *arf-3* mutant background. We do not disagree with the hypothesis that increased adhesion in these mutants prevents the cells from being shed, but propose that the increased adhesion results indirectly from a transformation of a cell fated to die into its surviving sister cell.

Our findings may provide insights into the mechanism of action of the Arf pathway in asymmetrically dividing cells. GRP-1 localization in midbodies is compatible with a function at the cleavage furrow during anaphase and cytokinesis, at a time when cell size asymmetry is established by spindle displacement in Q.p or myosin polarity in Q.a (Ou *et al.* 2010). We also previously proposed that *cnt-2* is required for endocytosis, in agreement with a requirement for GRP-1 at the plasma membrane (Singhvi *et al.* 2011). However, recent data indicate that CNT-2 and ARF-1.2 also function during the first division of the *C. elegans* embryo, and that CNT-2 is required to regulate cortical actomyosin dynamics (Fievet *et al.* 2012). Moreover, steppke, the *Drosophila* homolog of GRP-1, has been shown to antagonize myosin contractility at cleavage furrows in the cellularizing blastoderm (Lee and Harris 2013). Although the mechanism by which the Arf pathway controls daughter cell-size asymmetry remains unknown, it could involve the interplay of membrane trafficking and myosin contractility at the cleavage furrow or the asymmetric trafficking of polarity regulators or membrane to one pole of the cell.

Acknowledgments

We thank Yuji Kohara for providing *grp-1* cDNAs; Jon Audhya and Karen Oegema for the PLCδ1 cDNA; Sean O'Rourke and Bruce Bowerman for sharing GFP::EFA-6 reagents; Richard Ikegami for sharing the *gmIs65* transgene; Ofer Rog, Abby Dernburg, Guangshuo Ou, and Ron Vale for their help with time-lapse microscopy; and Shohei Mitani and the National Biosource Project and the Million Mutations Project for providing several of the mutants used in this study. Some nematode strains used in this work were provided by the *Caenorhabditis* Genetics Center, which is funded by the National Institutes of Health (NIH) Office of Research Infrastructure Programs (P40 OD010440). This work was supported by NIH grant NS32057 (G.G.). J.T. was supported by a fellowship from the Association pour la Recherche sur le Cancer.

Literature Cited

Baumeister, R., Y. Liu, and G. Ruvkun, 1996 Lineage-specific regulators couple cell lineage asymmetry to the transcription of the Caenorhabditis elegans POU gene unc-86 during neurogenesis. Genes Dev. 10: 1395–1410.

Branda, C. S., and M. J. Stern, 2000 Mechanisms controlling sex myoblast migration in Caenorhabditis elegans hermaphrodites. Dev. Biol. 226: 137–151.

Brenner, S., 1974 The genetics of Caenorhabditis elegans. Genetics 77: 71–94.

Bülow, H. E., and O. Hobert, 2004 Differential sulfations and epimerization define heparan sulfate specificity in nervous system development. Neuron 41: 723–736.

Casanova, J. E., 2007 Regulation of Arf activation: the Sec7 family of guanine nucleotide exchange factors. Traffic 8: 1476–1485.

Cherfils, J., J. Ménétrey, M. Mathieu, G. Le Bras, S. Robineau *et al.*, 1998 Structure of the Sec7 domain of the Arf exchange factor ARNO. Nature 392: 101–105.

Chien, S. C., E. M. Brinkmann, J. Teulière, and G. Garriga, 2013 *Caenorhabditis elegans* PIG-1/MELK acts in a conserved PAR-4/LKB1 polarity to promote asymmetric neuroblast divisions. Genetics 193: 897–909.

Clark, S. G., and C. Chiu, 2003 C. elegans ZAG-1, a Zn-finger-homeodomain protein, regulates axonal development and neuronal differentiation. Development 130: 3781–3794.

Cohen, L. A., A. Honda, P. Várnai, F. D. Brown, T. Balla *et al.*, 2007 Active Arf6 recruits ARNO/cytohesin GEFs to the PM by binding their PH domains. Mol. Biol. Cell 18: 2244–2253.

Conradt, B., and H. R. Horvitz, 1998 The C. elegans protein EGL-1 is required for programmed cell death and interacts with the Bcl-2-like protein CED-9. Cell 93: 519–529.

Cordes, S., C. A. Frank, and G. Garriga, 2006 The C. elegans MELK ortholog PIG-1 regulates cell size asymmetry and daughter cell fate in asymmetric neuroblast divisions. Development 133: 2747–2756.

Cowing, D. W., and C. Kenyon, 1992 Expression of the homeotic gene mab-5 during Caenorhabditis elegans embryogenesis. Development 116: 481–490.

Cronin, T. C., J. P. DiNitto, M. P. Czech, and D. G. Lambright, 2004 Structural determinants of phosphoinositide selectivity in splice variants of Grp1 family PH domains. EMBO J. 23: 3711–3720.

Denning, D. P., V. Hatch, and H. R. Horvitz, 2012 Programmed elimination of cells by caspase-independent cell extrusion in C. elegans. Nature 488: 226–230.

DiNitto, J. P., A. Delprato, M.-T. Gabe Lee, T. C. Cronin, S. Huang *et al.*, 2007 Structural basis and mechanism of autoregulation in 3-phosphoinositide-dependent Grp1 family Arf GTPase exchange factors. Mol. Cell 28: 569–583.

Donaldson, J. G., 2003 Multiple roles for Arf6: sorting, structuring, and signaling at the plasma membrane. J. Biol. Chem. 278: 41573–41576.

Donaldson, J. G., and C. L. Jackson, 2011 ARF family G proteins and their regulators: roles in membrane transport, development and disease. Nat. Rev. Mol. Cell Biol. 12: 362–375.

Ellis, H. M., and H. R. Horvitz, 1986 Genetic control of programmed cell death in the nematode C. elegans. Cell 44: 817–829.

Fievet, B. T., J. Rodriguez, S. Naganathan, C. Lee, E. Zeiser *et al.*, 2012 Systematic genetic interaction screens uncover cell polarity regulators and functional redundancy. Nat. Cell Biol. 15: 103–112.

Finney, M., G. Ruvkun, and H. R. Horvitz, 1988 The C. elegans cell lineage and differentiation gene unc-86 encodes a protein with a homeodomain and extended similarity to transcription factors. Cell 55: 757–769.

Frank, C. A., P. D. Baum, and G. Garriga, 2003 HLH-14 is a C. elegans achaete-scute protein that promotes neurogenesis through asymmetric cell division. Development 130: 6507–6518.

Frank, C. A., N. C. Hawkins, C. Guenther, H. R. Horvitz, and G. Garriga, 2005 C. elegans HAM-1 positions the cleavage plane and regulates apoptosis in asymmetric neuroblast divisions. Dev. Biol. 284: 301–310.

Frøkjær-Jensen, C., M. W. Davis, C. E. Hopkins, B. J. Newman, J. M. Thummel *et al.*, 2008 Single-copy insertion of transgenes in Caenorhabditis elegans. Nat. Genet. 40: 1375–1383.

Frøkjær-Jensen, C., M. W. Davis, M. Sarov, J. Taylor, S. Flibotte *et al.*, 2014 Random and targeted transgene insertion in Caenorhabditis elegans using a modified Mos1 transposon. Nat. Methods 11: 529–534.

Garriga, G., C. Desai, and H. R. Horvitz, 1993 Cell interactions control the direction of outgrowth, branching and fasciculation of the HSN axons of Caenorhabditis elegans. Development 117: 1071–1087.

Godi, A., P. Pertile, R. Meyers, P. Marra, G. Di Tullio *et al.*, 1999 ARF mediates recruitment of PtdIns-4-OH kinase-beta and stimulates synthesis of PtdIns(4,5)P2 on the Golgi complex. Nat. Cell Biol. 1: 280–287.

Guenther, C., and G. Garriga, 1996 Asymmetric distribution of the C. elegans HAM-1 protein in neuroblasts enables daughter cells to adopt distinct fates. Development 122: 3509–3518.

Gurling, M., K. Talavera, and G. Garriga, 2014 The DEP domain-containing protein TOE-2 promotes apoptosis in the Q lineage of C. elegans through two distinct mechanisms. Development 141: 2724–2734.

Hatzold, J., and B. Conradt, 2008 Control of apoptosis by asymmetric cell division. PLoS Biol. 6: e84.

Hawkins, N. C., G. C. Ellis, B. Bowerman, and G. Garriga, 2005 MOM-5 frizzled regulates the distribution of DSH-2 to control C. elegans asymmetric neuroblast divisions. Dev. Biol. 284: 246–259.

Hirose, T., and H. R. Horvitz, 2013 An Sp1 transcription factor coordinates caspase-dependent and -independent apoptotic pathways. Nature 500: 354–358.

Hofmann, I., A. Thompson, C. M. Sanderson, and S. Munro, 2007 The Arl4 family of small G proteins can recruit the cytohesin Arf6 exchange factors to the plasma membrane. Curr. Biol. 17: 711–716.

Honda, A., M. Nogami, T. Yokozeki, M. Yamazaki, H. Nakamura *et al.*, 1999 Phosphatidylinositol 4-phosphate 5-kinase alpha is a downstream effector of the small G protein ARF6 in membrane ruffle formation. Cell 99: 521–532.

Hsu, D. R., P. T. Chuang, and B. J. Meyer, 1995 DPY-30, a nuclear protein essential early in embryogenesis for Caenorhabditis elegans dosage compensation. Development 121: 3323–3334.

Jackson, T. R., B. G. Kearns, and A. B. Theibert, 2000 Cytohesins and centaurins: mediators of PI 3-kinase-regulated Arf signaling. Trends Biochem. Sci. 25: 489–495.

Jones, D. H., J. B. Morris, C. P. Morgan, H. Kondo, R. F. Irvine *et al.*, 2000 Type I phosphatidylinositol 4-phosphate 5-kinase directly interacts with ADP-ribosylation factor 1 and is responsible for phosphatidylinositol 4,5-bisphosphate synthesis in the golgi compartment. J. Biol. Chem. 275: 13962–13966.

Kahn, R. A., J. Cherfils, M. Elias, R. C. Lovering, S. Munro *et al.*, 2006 Nomenclature for the human Arf family of GTP-binding proteins: ARF, ARL, and SAR proteins. J. Cell Biol. 172: 645–650.

Kamath R. S., M. Martinez-Campos, P. Zipperlen, A. G. Fraser, J. Ahringer, 2001 Effectiveness of specific RNA-mediated interference through ingested double-stranded RNA in Caenorhabditis elegans. Genome Biol. 2: RESEARCH0002.

Kennedy, S., D. Wang, and G. Ruvkun, 2004 A conserved siRNA-degrading RNase negatively regulates RNA interference in C. elegans. Nature 427: 645–649.

Kim, K., and C. Li, 2004 Expression and regulation of an FMRFamide-related neuropeptide gene family in Caenorhabditis elegans. J. Comp. Neurol. 475: 540–550.

Kiyomitsu, T., and I. M. Cheeseman, 2013 Cortical dynein and asymmetric membrane elongation coordinately position the spindle in anaphase. Cell 154: 391–402.

Klarlund, J. K., W. Tsiaras, J. J. Holik, A. Chawla, and M. P. Czech, 2000 Distinct polyphosphoinositide binding selectivities for pleckstrin homology domains of GRP1-like proteins based on diglycine *vs.* triglycine motifs. J. Biol. Chem. 275: 32816–32821.

Kolanus, W., 2007 Guanine nucleotide exchange factors of the cytohesin family and their roles in signal transduction. Immunol. Rev. 218: 102–113.

Kolanus, W., W. Nagel, B. Schiller, L. Zeitlmann, S. Godar *et al.*, 1996 Alpha L beta 2 integrin/LFA-1 binding to ICAM-1 induced by cytohesin-1, a cytoplasmic regulatory molecule. Cell 86: 233–242.

Kreis, T. E., M. Lowe, and R. Pepperkok, 1995 COPs regulating membrane traffic. Annu. Rev. Cell Dev. Biol. 11: 677–706.

Lee, D. M., and T. J. C. Harris, 2013 An Arf-GEF regulates antagonism between endocytosis and the cytoskeleton for Drosophila blastoderm development. Curr. Biol. 23: 2110–2120.

Li, C., K. Kim, and L. S. Nelson, 1999 FMRFamide-related neuropeptide gene family in Caenorhabditis elegans. Brain Res. 848: 26–34.

Li, C.-C., T.-C. Chiang, T.-S. Wu, G. Pacheco-Rodriguez, J. Moss *et al.*, 2007 ARL4D recruits cytohesin-2/ARNO to modulate actin remodeling. Mol. Biol. Cell 18: 4420–4437.

Li, Y., W. G. Kelly, J. M. Logsdon, A. M. Schurko, B. D. Harfe *et al.*, 2004 Functional genomic analysis of the ADP-ribosylation factor family of GTPases: phylogeny among diverse eukaryotes and function in C. elegans. FASEB J. 18: 1834–1850.

Liang, J. O., and S. Kornfeld, 1997 Comparative activity of ADP-ribosylation factor family members in the early steps of coated vesicle formation on rat liver Golgi membranes. J. Biol. Chem. 272: 4141–4148.

Maduro, M., and D. Pilgrim, 1995 Identification and cloning of unc-119, a gene expressed in the Caenorhabditis elegans nervous system. Genetics 141: 977–988.

Moss, J., and M. Vaughan, 2002 Cytohesin-1 in 2001. Arch. Biochem. Biophys. 397: 156–161.

Mossessova, E., J. M. Gulbis, and J. Goldberg, 1998 Structure of the guanine nucleotide exchange factor Sec7 domain of human arno and analysis of the interaction with ARF GTPase. Cell 92: 415–423.

Nakai, K., and P. Horton, 1999 PSORT: a program for detecting sorting signals in proteins and predicting their subcellular localization. Trends Biochem. Sci. 24: 34–36.

Nie, Z., D. S. Hirsch, and P. A. Randazzo, 2003 Arf and its many interactors. Curr. Opin. Cell Biol. 15: 396–404.

O'Rourke, S. M., S. N. Christensen, and B. Bowerman, 2010 Caenorhabditis elegans EFA-6 limits microtubule growth at the cell cortex. Nat. Cell Biol. 12: 1235–1241.

Ou, G., N. Stuurman, M. D'Ambrosio, and R. D. Vale, 2010 Polarized myosin produces unequal-size daughters during asymmetric cell division. Science 330: 677–680.

Popoff, V., J. D. Langer, I. Reckmann, A. Hellwig, R. A. Kahn *et al.*, 2011 Several ADP-ribosylation factor (Arf) isoforms support COPI vesicle formation. J. Biol. Chem. 286: 35634–35642.

Potts, M. B., and S. Cameron, 2011 Cell lineage and cell death: Caenorhabditis elegans and cancer research. Nat. Rev. Cancer 11: 50–58.

Randazzo, P. A., Z. Nie, K. Miura, and V. W. Hsu, 2000 Molecular aspects of the cellular activities of ADP-ribosylation factors. Sci. STKE 2000: re1.

Rual, J.-F., J. Ceron, J. Koreth, T. Hao, A.-S. Nicot *et al.*, 2004 Toward improving Caenorhabditis elegans phenome mapping with an ORFeome-based RNAi library. Genome Res. 14: 2162–2168.

Salser, S. J., and C. Kenyon, 1992 Activation of a C. elegans Antennapedia homologue in migrating cells controls their direction of migration. Nature 355: 255–258.

Shaham, S., P. W. Reddien, B. Davies, and H. R. Horvitz, 1999 Mutational analysis of the Caenorhabditis elegans cell-death gene ced-3. Genetics 153: 1655–1671.

Simmer, F., M. Tijsterman, S. Parrish, S. P. Koushika, M. L. Nonet *et al.*, 2002 Loss of the putative RNA-directed RNA polymerase RRF-3 makes C. elegans hypersensitive to RNAi. Curr. Biol. 12: 1317–1319.

Singhvi, A., J. Teulière, K. Talavera, S. Cordes, G. Ou *et al.*, 2011 The Arf GAP CNT-2 regulates the apoptotic fate in C. elegans asymmetric neuroblast divisions. Curr. Biol. 21: 948–954.

Stalder, D., H. Barelli, R. Gautier, E. Macia, C. L. Jackson *et al.*, 2011 Kinetic studies of the Arf activator Arno on model membranes in the presence of Arf effectors suggest control by a positive feedback loop. J. Biol. Chem. 286: 3873–3883.

Sze, J. Y., S. Zhang, J. Li, and G. Ruvkun, 2002 The C. elegans POU-domain transcription factor UNC-86 regulates the tph-1 tryptophan hydroxylase gene and neurite outgrowth in specific serotonergic neurons. Development 129: 3901–3911.

Timmons, L., and A. Fire, 1998 Specific interference by ingested dsRNA. Nature 395: 854.

Várnai, P., T. Bondeva, P. Tamás, B. Tóth, L. Buday *et al.*, 2005 Selective cellular effects of overexpressed pleckstrin-homology domains that recognize PtdIns(3,4,5)P3 suggest their interaction with protein binding partners. J. Cell Sci. 118: 4879–4888.

Volpicelli-Daley, L. A., Y. Li, C.-J. Zhang, and R. A. Kahn, 2005 Isoform-selective effects of the depletion of ADP-ribosylation factors 1–5 on membrane traffic. Mol. Biol. Cell 16: 4495–4508.

Wicks, S. R., R. T. Yeh, W. R. Gish, R. H. Waterston, and R. H. Plasterk, 2001 Rapid gene mapping in Caenorhabditis elegans using a high density polymorphism map. Nat. Genet. 28: 160–164.

Communicating editor: P. Sengupta

GENETICS

Supporting Information
http://www.genetics.org/lookup/suppl/doi:10.1534/genetics.114.167189/-/DC1

Asymmetric Neuroblast Divisions Producing Apoptotic Cells Require the Cytohesin GRP-1 in *Caenorhabditis elegans*

Jerome Teuliere, Shaun Cordes, Aakanksha Singhvi, Karla Talavera, and Gian Garriga

DOI: 10.1534/genetics.114.167189

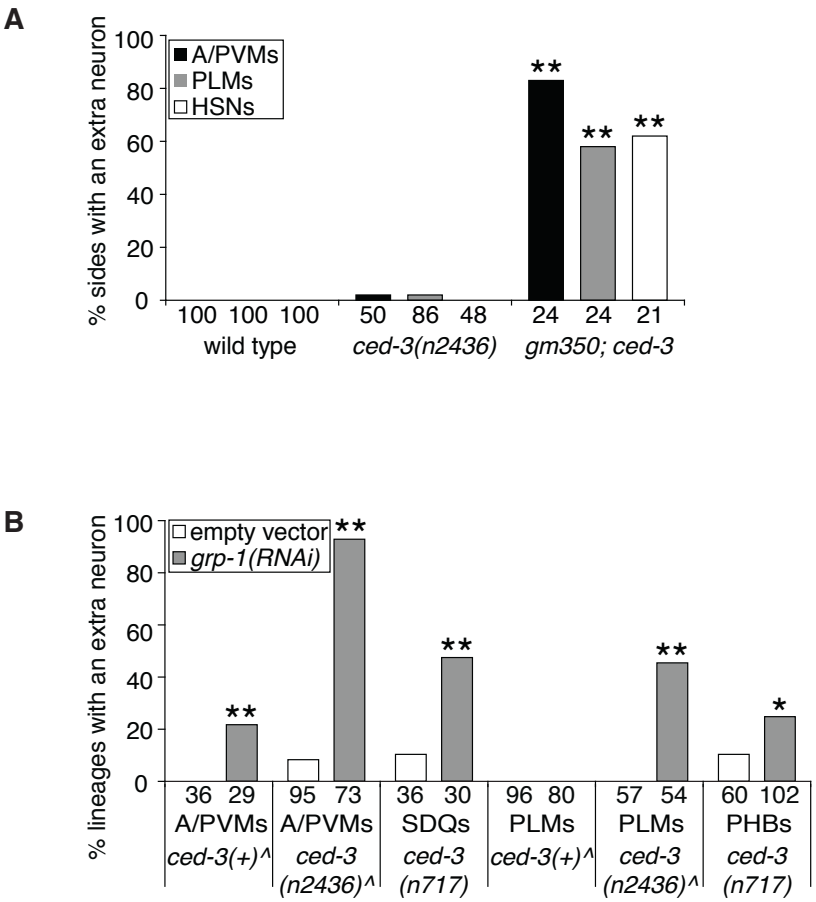

Figure S1 *grp-1* mutant and RNAi phenotypes. (A) Extra neuron defects in the original *gm350; ced-3* strain isolated from the screen for mutants with extra A/PVMs, compared to the basal level of extra neurons in the *ced-3(n2436)* hypomorphic mutant. (B) Reducing *grp-1* activity by RNAi phenocopies the *grp-1(gm350)* and *grp-1; ced-3* mutant phenotypes in the Q.p and ALN/PLM neuroblast lineages. Control (empty vector) and *grp-1* RNAi treatments were performed in wild-type *ced-3 (+)* and *ced-3* mutant backgrounds. Worm strains used in the RNAi experiments that contained an RNAi-sensitizing mutation in *rrf-3* are indicated with a ^ (SIMMER *et al*. 2002). The number of lineages scored per genotype is shown under each bar. * $p < 0.05$, ** $p < 0.005$.

A

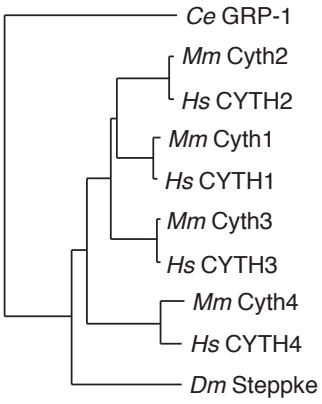
Ce GRP-1
Mm Cyth2
Hs CYTH2
Mm Cyth1
Hs CYTH1
Mm Cyth3
Hs CYTH3
Mm Cyth4
Hs CYTH4
Dm Steppke

B

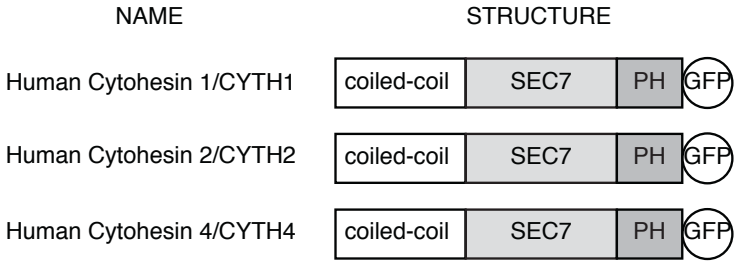
NAME
STRUCTURE
Human Cytohesin 1/CYTH1
Human Cytohesin 2/CYTH2
Human Cytohesin 4/CYTH4
coiled-coil
SEC7
PH
GFP

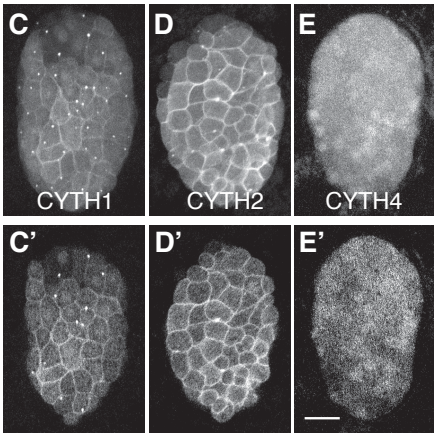
C
D
E
CYTH1
CYTH2
CYTH4
C'
D'
E'

F

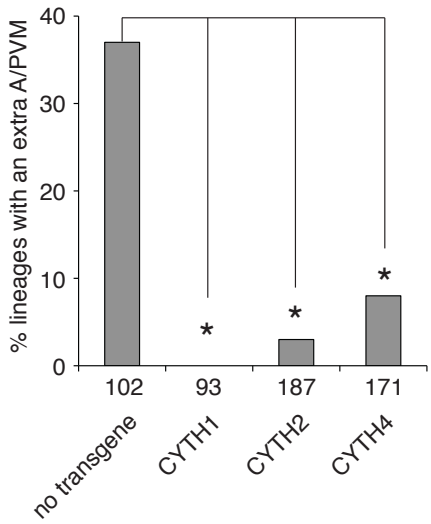
% lineages with an extra A/PVM
40
30
20
10
0
102
93
187
171
no transgene
CYTH1
CYTH2
CYTH4
*
*
*

Figure S2 Human cytohesins can compensate for *grp-1* loss. (A) Phylogenetic relationships among cytohesins from human (Hs), mouse (Mm), Drosophila (Dm) and *C.elegans* (Ce). (B) Diagrams of the cytohesin-GFP constructs used. CYTH1, CYTH2 and CYTH4 are human cytohesins. All constructs were expressed from the *dpy-30* promoter, which drives broad expression. (C-E') Localization of human cytohesins GFP fusions in *C. elegans* embryos. (C-E) Confocal projections. (C'-E') Individual slices from the related confocal series. CYTH 1 and 2 localized to nuclei, to the cytoplasm and at the cell periphery whereas CYTH4 localized to the cytoplasm and nuclei. Scale bar, 10 μm. (F) Ability of the different transgenes to rescue the A/PVM phenotype of *grp-1(gm350)* mutants. The number of lineages scored per genotype is shown under each bar. NS not significant, * $p < 0.0001$.

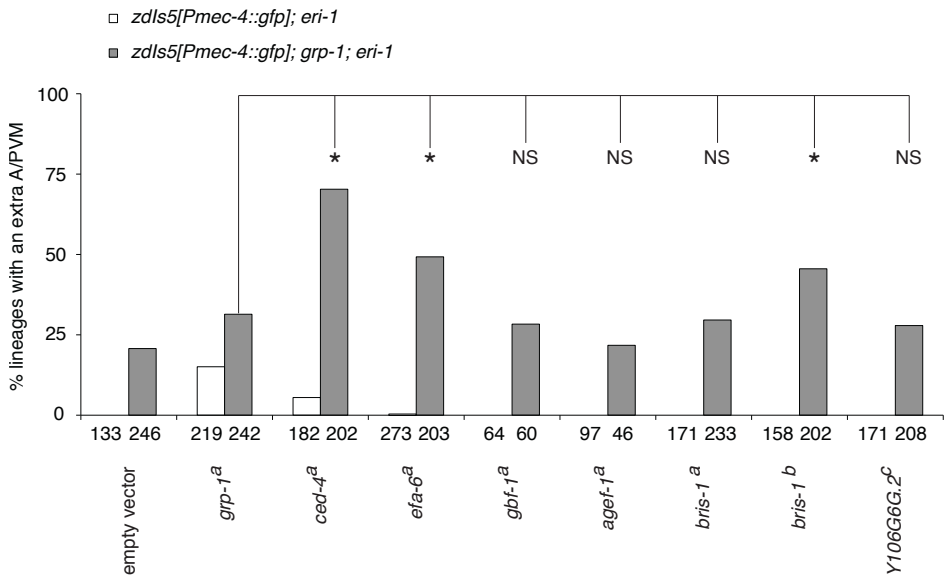

Figure S3 Arf GEF RNAi enhancer screen. RNAi clones targeting the Arf GEF genes *efa-6* and *bris-1*, but not other Arf GEF genes, enhanced the *grp-1(gm350)* mutant A/PVM phenotype. *Arf GEF(RNAi)* was performed in wild-type *grp-1(+)* (white bars) and *grp-1(gm350)* mutant (grey bars) backgrounds that contained an RNAi-sensitizing mutation in *eri-1* (KENNEDY *et al.* 2004). We observed a reduced penetrance of the extra-neuron phenotype in the mock-treated *grp-1; eri-1* double mutant, and used worms treated with the *grp-1* RNAi clone as a more stringent reference. *ced-4(RNAi)* provided a positive control for the RNAi experiment. Clones were (a) from (KAMATH *et al.* 2001); (b) from (RUAL *et al.* 2004); or (c) constructed for this study. Results shown represent cumulative data of at least three independent experiments for each clone. The total number of lineages scored is shown under each bar. NS not significant, * $p < 0.0001$.

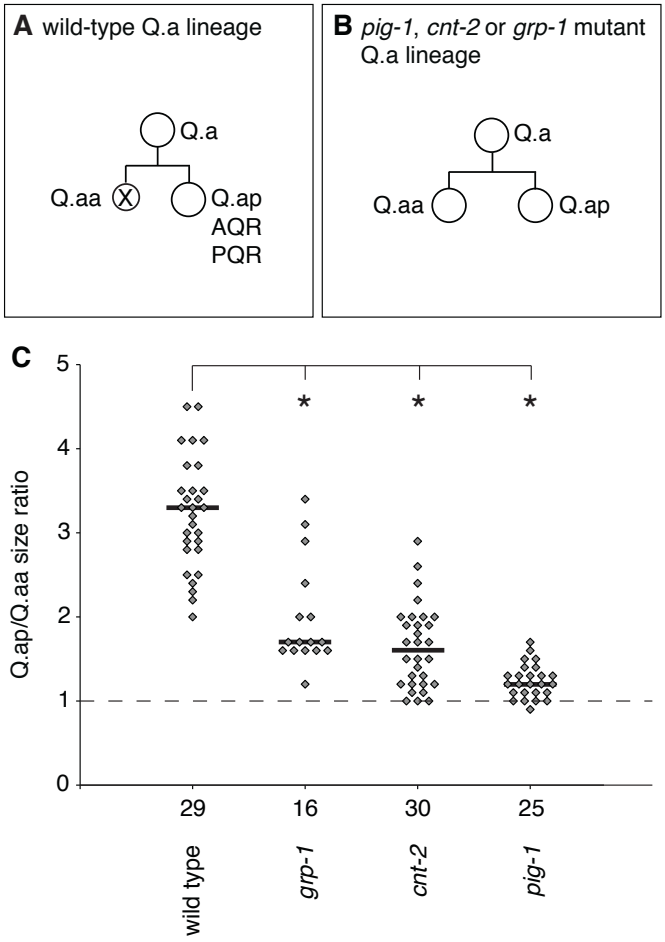

Figure S4 GRP-1 and CNT-2 regulate Q.a daughter cells size asymmetry.
(A) The wild-type Q.a neuroblast division produces one neuron (A/PQR) and a smaller dying cell (Q.aa). (B) The Q.a division of *pig-1, cnt-2* and *grp-1* mutants produce daughters that are more equivalent in size, and the anterior daughter can sometimes survive, and adopt its sister's A/PQR neuronal fate. The *pig-1* Q.a phenotype was previously described by Ou and colleagues (Ou *et al.* 2010) (C) Q.ap/Q.aa ratio. Each dot corresponds to the size ratio of one pair of Q.a daughters, and the horizontal bars indicate the median of the ratio distribution. The dashed horizontal line indicates a 1:1 ratio corresponding to Q.a daughter cells of equivalent sizes. * $P < 0.001$.

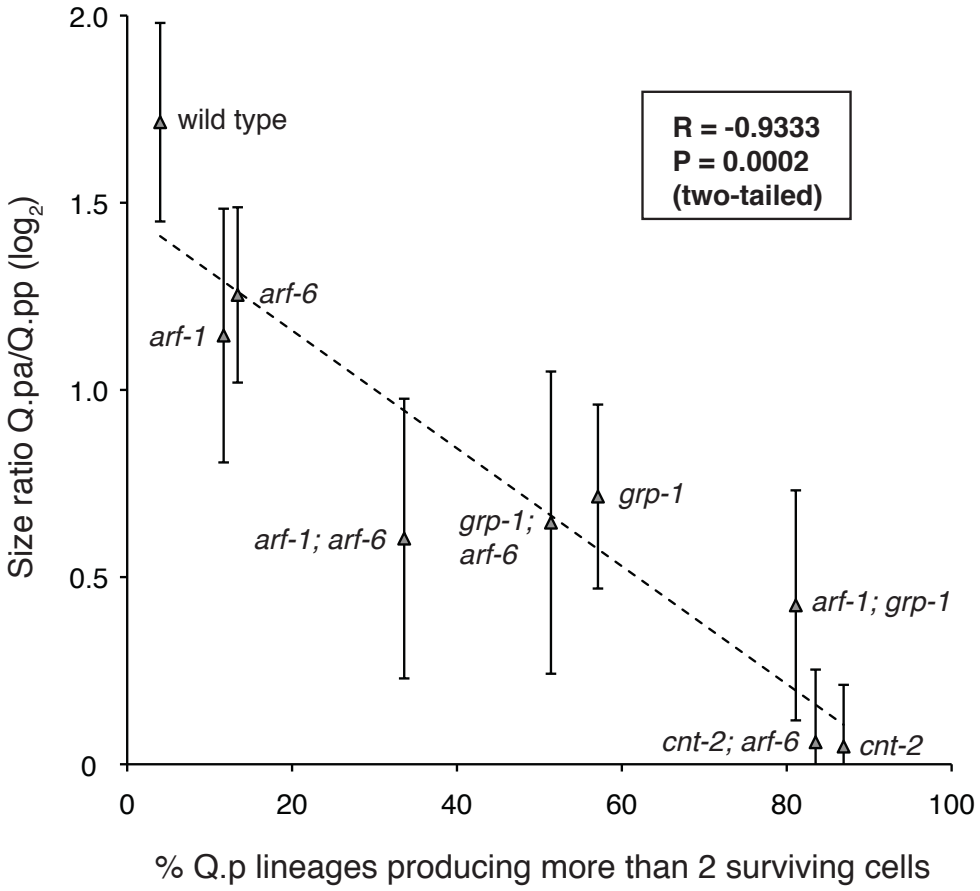

Figure S5 Correlation between the Q.pa/Qpp cell size ratio (log2 representation) and the percent of Q.p lineages that produce extra surviving cells. Triangles indicate the mean ratio for each genotype indicated (distributions are shown in Figure 4C, n=9 genotypes). Error bars indicate standard deviation. The linear regression (dashed line) and the Pearson correlation coefficient (R) and P-value (P) are indicated on the graph.

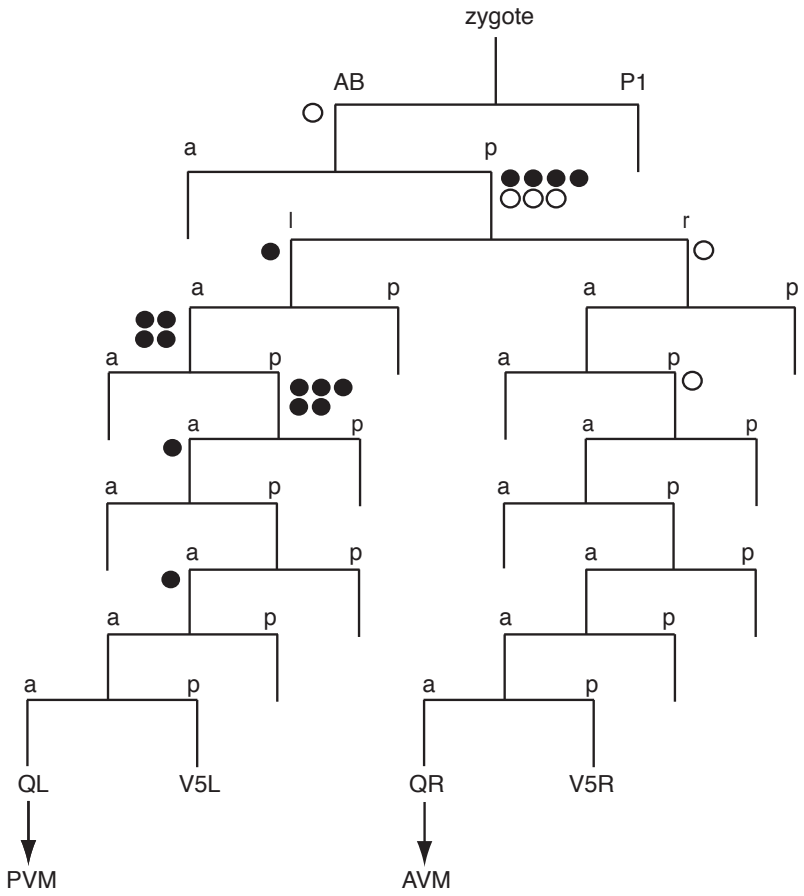

Figure S6 Mosaic analysis of *grp-1* function for the extra A/PVM phenotype. The lineage tree is a schematic diagram of the part of the *C. elegans* lineage that gives rise to the AVM and PVM neurons. Abbreviations: a, anterior; p, posterior; l, left; r, right. *zdIs5* [*mec-4::gfp*]; *grp-1(gm350)* mutants mosaic for *gmEx353* [*grp-1(+); Pdpy-30::NLS::DsRed2*] were screened for the presence of extra AVMs and PVMs using *zdIs5*. Animals that had an extra neuron were scored using the DsRed2 marker to identify in which cells the array had been lost. Filled circles indicate array losses that generated an extra PVM. Empty circles indicate array losses that generated an extra AVM.

File S1

Plasmid construction

All DNA sequences are provided in 5' to 3' orientation. Capital letters are used to indicate the positions of restriction enzyme sites engineered into PCR primers, and the locations of nucleotide mismatches in primers used for site-directed mutagenesis. Several PCR products were cloned using the Zero Blunt TOPO PCR Cloning Kit (Invitrogen), which will be referred to as TOPO cloning. Directed mutagenesis was performed using the QuikChange II XL Site-Directed Mutagenesis Kit (Stratagene).

To construct a plasmid (bGG836) containing the *grp-1* genomic region [*grp-1(+)*], we used primers *grp-1A* [catcggttctggaaagcttatt] and *grp-1B* [ggttcaacaccttgcaaaaa] to amplify a 3.6 kb fragment of the genomic region spanning from the end of the gene upstream of *grp-1* to the beginning of the immediate downstream gene. The PCR product was TOPO cloned to yield plasmid bGG836.

To construct *Pgrp-1::gfp::grp-1* (SC-84), we first amplified from bGG836 a 770 bp DNA fragment containing the *grp-1* promoter (the intergenic region between *grp-1* and the gene immediately upstream) using primers *grp1-3* [aaCGGCCGcatcggttctggaaagcttatt] and *grp1-4* [aaGGTACCatttatcccttgtttttccgc]. The 2.3 kb *grp-1* genomic region was amplified using primers *grp1-1* [aaGCTAGCatgtcatcgcggtattcagg] and *grp1-2* [aaTCCGGAtcagtgggtacttttggtc], which contain *Nhe*I and *BspE*I sites, respectively. Both PCR products were TOPO cloned to generate plasmids SC-65 (*grp-1* promoter) and SC-69 (*grp-1* ORF). The *grp-1* promoter was then subcloned into the GFP vector pPD118.15 (Addgene, Cambridge, MA) upstream of the sequences encoding GFP using *Eag*I and *Acc65*I. The *grp-1* genomic region was subcloned into the resulting plasmid downstream and in frame with GFP using *Nhe*I and *BspE*I to generate plasmid SC-84.

To construct *Pmab-5::grp-1::gfp* (SC-79), we amplified a full length *grp-1* cDNA from an oligo-d(T)-primed cDNA library (a gift of Lianna Wong) using primers *grp1cDNA-F* [ttCCCGGGatgtcatcgcggtattcaga] and *grp1cDNA-R* [ttCCCGGGtgggtacttttggtctgg]. The cDNA was TOPO cloned to generate SC-67, and then subcloned into plasmid *pPD95.77::Pmab-5* using XmaI to yield SC-79. *pPD95.77::Pmab-5* contains an 8.8 kb genomic fragment containing the *mab-5* promoter upstream of sequences encoding GFP (FLEMING *et al.* 2005), and the *grp-1* cDNA was subcloned downstream of the *mab-5* promoter and in-frame with GFP.

To construct *Pdpy-30::grp-1::gfp* (SC-94), we amplified a ~800 bp fragment containing the *dpy-30* promoter from plasmid SC-73 [*Pdpy-30::NLS::DsRed2*] using primers *grp1-11* [tAAGCTTctatagggcgaattggagct] and *grp1-12* [tCTGCAGtcttggtttttgctcgatttct], and the resulting product was TOPO cloned to generate plasmid SC-92. A full-length *grp-1* cDNA was amplified from plasmid SC-67 using primers *grp1-13* [tGTCGACatgtcatcgcggtattcaga] and *grp1-14* [tGGTACCgcgtgggtacttttggtctgg]. This product was TOPO cloned, yielding plasmid SC-91. The *dpy-30* promoter was then subcloned from SC-92 into vector pPD95.77 upstream of sequences encoding GFP using *Hind*III and *Pst*I sites engineered into the *grp1-11* and *grp1-12* primers, respectively. The resulting plasmid, SC-93, was used as the vector into which the *grp-1* cDNA was subcloned from SC-91 using *Sal*I and *Acc65*I sites located in the *grp1-13* and *grp1-14* primers, respectively, to generate the SC-94 plasmid.

To construct *Pdpy-30::grp-1mutNLS::gfp* (SC-104), we mutated the putative grp-1 NLS in SC-91 from PKVRKRK to PKVAARK using primers grp1-17 [gatgactcttcccaaagtaGCcGCCaggaaggcacaacttgtcgatg] and grp1-18 [catcgacaagttgtgccttcctGGCgGCtactttgggaagagtcatc] and generate the plasmid SC-97. The mutated cDNA was then subcloned into SC-93 using *Sal*I and *Acc65*I.

To construct *Pdpy-30::NES-grp-1::gfp* (SC-106), we amplified a *grp-1* cDNA from plasmid SC-67 using primers grp1-14 and grp1-15 [tGTCGACatgcttgcccttaagctcgccggacttgatattatgtcatcgcggtattcaga]. grp1-15 contains a sequence encoding the peptide LALKLAGLDI which is the nuclear export signal (NES) of heat-stable protein kinase inhibitor (PKI) [1]. The amplified product was TOPO cloned to generate the SC-101 plasmid, and subcloned from SC-101 into SC-93 [*Pdpy-30::gfp*] using *Sal*I and *Acc65*I sites located in the grp1-15 and grp1-14 primers, respectively.

To construct *Pdpy-30::MYR::grp-1::gfp* (SC-102) and *Pdpy-30::MYR::grp-1(mutNLS)::gfp* (SC-116), we annealed primers grp1-20 [TCGAatgggatcttccaagtcta] and grp1-21 [TCGAtagacttggaagatcccat] together and ligated the resulting double-stranded DNA into *Sal*I-digested SC-94 and SC-104, respectively, between the promoter and *grp-1* sequences.

To construct *Pdpy-30::GRP-1K270A::gfp* (SC-128), we mutated the PH domain encoded by the *grp-1* cDNA in SC-91 using primers K270A-F [acgagaaggatggcttttcgcgcagagtagtaatcc] and K270A-R [ggattactactctgcgcgaaaagccatccttctcgt] to generate SC-122. The mutated cDNA was then subcloned into SC-93 using *Sal*I and *Acc65*I sites.

To construct *Pdpy-30::GRP-1CC::gfp* (pAS1) we amplified the corresponding first 174 bp from *grp-1* cDNA using primers grp-1-CC-F1 [aaaGTCGACatgtcatcgcggtat] and grp-1-CC-R1 [ttcGGTACCgcttttgattttgg], containing restriction sites for *Sal*I and *Acc65*I enzymes. The mutated cDNA was then subcloned into SC-93 using *Sal*I and *Acc65*I sites.

To construct *Pdpy-30::GRP-1E155K::gfp* (SC-127), we mutated the SEC7 domain encoded by the *grp-1* cDNA in SC-91 using primers E155K-F [ttccggctacctggcaaatcgaaaattaatc] and E155K-R [gattaattttctgcgatttgccaggtagccggaa] to generate SC-120. The mutated cDNA was then subcloned into SC-93 using *Sal*I and *Acc65*I sites.

To construct *Pdpy-30::GRP-1SEC7::gfp* (SC-126) we amplified the corresponding 575 bp from *grp-1* cDNA using primers grp-1-SEC7-F1 [aggGTCGACgaatatcacaaa] and grp-1-SEC7-R1 [ttcGGTACCgcacttgtcgatac], containing restriction sites for *Sal*I and *Acc65*I enzymes. The amplified product was TOPO cloned to generate the SC-119 plasmid, and subcloned into SC-93 using *Sal*I and *Acc65*I sites.

To generate mRFP::SEC7::GFP fusions, mRFP was first amplified from using primers mRFP-F [tGTCGACatggcctcctccgaggacgt] and mRFP-stop [ttGAATTCctattaggcgccggtggagtg], and TOPO cloned to generate the SC-145 plasmid, or using primers mRFP-F and grp1-24 [tAGATCTggcgccggtggagtggcggc], and cloned similarly to generate the SC-144 plasmid, or amplified with a SV40 NLS using primers grp1-24 and grp1-26 [tGTCGACatgactgctccaaagaagaagcgtaaggtaatggcctcctccgaggacgt], and cloned similarly to generate the SC-111 plasmid. The mRFP insert from SC-145 was subcloned into SC-93 using *Sal*I and *EcoR*I sites to generate the SC-146 plasmid. The *grp-1* PH domain was amplified from SC-91 using primers grp1-14 and grp1-25 [tAGATCTaagatcccagatgaagtatc] and TOPO cloned to generate the SC-112 plasmid.
The mRFP insert from SC-111 and the PH domain insert from SC-112 were subcloned in a trimolecular ligation into SC-93 using the *Acc65*I, *Bgl*II and *Sal*I sites to generate the plasmid SC-118.
Finally, the *grp-1* SEC7 domain was amplified using primers SEC7-BglII [tAGATCTacccatccaaaatcaaaaga] and grp-1-SEC7-R1, then TOPO cloned to generate the SC-140 plasmid.

To construct *Pdpy-30::mRFP::GRP-1SEC7::gfp* (SC-151), the mRFP insert from SC-144 and the SEC7 domain from SC-140 were subcloned into SC-93 in a trimolecular ligation using the *Sal*I, *Acc65*I and *Bgl*II sites.

To construct *Pdpy-30::NLS::mRFP::GRP-1SEC7::gfp* (SC-147), the SEC7 domain from SC-140 were subloned into SC-118 using the *Acc65*I and *Bgl*II sites.

To construct *Pdpy-30::PLCdelta1PH::mRFP::GRP-1SEC7::gfp* (SC-159), the cDNA encoding the rat phospholipase C delta 1 PH domain was amplfied from pAA1 (a gift from Jon Audhya and Karen Oegema) using primers PLCPH-F [tGTCGACatgcacgggctccaggatgac] and PLCPH-R [tGTCGACcttctgccgctggtccatg], then subcloned into SC-151 using the introduced *Sal*I sites.

To construct *Pdpy-30::CYTH1::gfp* (SC-148), *Pdpy-30::CYTH2::gfp* (SC-149) and *Pdpy-30::CYTH4::gfp* (SC-160), the respective human cytohesins were amplified from ATCC human cDNA clones (http://www.atcc.org/) using primers CYTH1-F [tGTCGACatggaggaggacgacagcta] and CYTH1-R [tGGTACCgcgtgtcgcttcgtggaggaga], CYTH2-F [tGTCGACatggaggacggcgtctatga] and CYTH2-R [tggtaccgcgggctgctcctgcttcttct], CYTH4-F [tGTCGACatggacctgtgccacccaga] and CYTH4-R [tGGTACCgcctgcttgctggcaatcttcttc], then TOPO cloned to generate the SC-131, SC-133 and SC-132 plasmids, respectively. Each cDNA was then subcloned into SC-93 using the *Sal*I and *Acc65*I sites.

To construct a Y106G6G.2 RNAi clone, we amplified a Y106G6G.2 524 bp fragment from *C. elegans* genomic DNA using primers Y106G6G.2E [ttGAATTCgtgtgcttgcttttccaggg] and Y106G6G.2F [ttGAATTCgcaacaattgtcttgactgcg] and cloned it into the L4440 plasmid using *EcoR*I sites.

To construct *arl-6* and *arl-13* RNAi clones, we amplified cDNA sequences using a *C. elegans* embryonic cDNA library as template. Primers used were ARL6F [atgggcttcttttcgtcattgtcc] and ARL6R [tccaatccatctccagtgagtgc] for *arl-6* and ARL13F [atgaccgaaaagtcgtggttcga] ARL13R [cgttttgaatcctttgtatccggct] for *arl-13*. These fragments when then cloned into the L4440 plasmid using *EcoR*V sites.

Mos1-mediated Single Copy Insertion (MosSCI) clones were engineered by Multisite Gateway Cloning (Invitrogen) recombination of promoter, cDNA and unc-54 3'UTR (pJT9) pENTR plasmids into the MosSCI vector pCFJ150 (FRØKJÆR-JENSEN *et al.* 2008). The pENTR clones construction is described below (attB sites are upper case).

pENTR *unc-54* 3'UTR (pJT9): *unc-54* 3'UTR was amplified from genomic DNA using primers B2unc-54B3-F [ggggACAGCTTTCTTGTACAAAGTGGcatctcgcgcccgtgcctct] and B2unc-54B3-R [ggggACAACTTTGTATAATAAAGTTGaaacagttatgtttggtatattgggaatgtattct], then recombined into pDONR P2RP3.

pENTR *pmab-5* (#bgg1127): the *mab-5* promoter was amplified from pPD95.77 *Pmab-5* using primers B4pmab-5B1-F [ggggACAACTTTGTATAGAAAAGTTGaagcttgattcagggtggtcgaca] and B4pmab-5B1-R [ggggACTGCTTTTTTGTACAAACTTGaatattttagttattaagattcca], then recombined into pDONR P4P1R.

pENTR *punc-86* (#bgg1126): the *unc-86* promoter was amplified from genomic DNA using primers B4punc-86B1-F [ggggACAACTTTGTATAGAAAAGTTGccactagtttctagtgaataaatcccc] and B4punc-86B1-R [ggggACTGCTTTTTTGTACAAACTTGcgtccgtggaaaagaggg], then recombined into pDONR P4P1R.

pENTR *grp-1::gfp* (pJT43): *grp-1::gfp* was amplified from SC-79 using primers B1grp-1gfpB2-F [ggggACAAGTTTGTACAAAAAAGCAGGCTatgtcatcgcggtattcagaacg] and B1gfpB2-R [ggggACCACTTTGTACAAGAAAGCTGGGTctatttgtatagttcatccatgccatgtgta], then recombined into pDONR 221.

pENTR *arf-6::gfp* (pJT44): *arf-6* was amplified from TOPO cloned *arf-6* cDNA using primers B1arf-6B2-F [ggggACAAGTTTGTACAAAAAAGCAGGCTatgggtaaattcctgtcgaaaatct] and arf-6gfpR [tgaaaagttcttctcctttactcatcggcttgcaattctggcttagccac], and gfp was amplified from Pmab-5::cnt-2::gfp (Singhvi et al, 2011) using primers arf-6gfp-F[gtggctaagccagaattgcaagccgATGAGTAAAGGAGAAGAACTTTTCA] and B1gfpB2-R, then the two fragments were PCR-fused and the *arf-6::gfp* cDNA was amplified using B1arf-6B2-F and B1gfpB2-R, and finally recombined into pDONR 221.

pENTR *cnt-2::gfp* (pJT48): *cnt-2::gfp* was amplified from Pmab-5::cnt-2::gfp [3] using primers B1cnt-2gfpB2-F [ggggACAAGTTTGTACAAAAAAGCAGGCTatgtcgcgacacctactaacagg] and B1gfpB2-R, then recombined into pDONR 221.

pENTR *gfp::efa-6* (pJT77): *gfp::efa-6a* cDNA was amplified from *Ppie-1::gfp::efa-6a* [4] using primers B1gfpB2-F [ggggACAAGTTTGTACAAAAAAGCAGGCTatgagtaaaggagaagaacttttcactgga] and B1efa-6B2-R [ggggACCACTTTGTACAAGAAAGCTGGGTtcaatgagcagcagctccattaacagc], then recombined into pDONR 221.

pENTR *gfp::efa-6E447K* (pJT102): pJT77 was mutagenized using the primers efa-6E447K-F [tccgtggtaaatcatcagctcgtgaacgtttgctc] and efa-6E447K-R [gctgatgaTTTaccacggagctctactcggctcaa].

pENTR *gfp::efa-6ΔMTR* (pJT103): pJT77 was mutagenized using the primers efa-6delMTR-F [gagcccctcgccggaatgtcaacgtttcgagcacttatgcaaagcttctcggc] and efa-6delMTR-R [gcataagtgctcgaaacgttgacattccggcgaggggctccatcaatggtggc].

The reactions were performed using pCFJ150 and pJT9 as well as the following pENTR clones:

- *Pmab-5::arf-6::GFP* (pJT122): #bgg1127, pJT44.
- *Punc-86::grp-1::GFP* (pJT50): #bgg1126, pJT43.
- *Punc-86::cnt-2b::GFP* (pJT49): #bgg1126, pJT48.
- *Pmab-5::GFP::EFA-6* (pJT101): #bgg1127, pJT77.
- *Pmab-5::GFP::EFA-6 E447K* (pJT107): #bgg127, pJT102.
- *Pmab-5::GFP::EFA-6 ΔMTR* (pJT106): #bgg127, pJT103.

Table S1 DNA constructs and transgenes used in this study

Transgenes used	Description	DNA constructs injected (concentrations in ng/μl)
gmEx361 *gmEx363*	GFP::GRP-1 *Pgrp-1::gfp::grp-1*	SC-84 (10), pRF4 (40)
gmEx462	CYTH1 *Pdpy-30::CYTH1-GFP*	SC-148 (10), pRF4 (50)
gmEx464	CYTH2 *Pdpy-30::CYTH2-GFP*	SC-149 (10), pRF4 (50)
gmEx466	CYTH4 *Pdpy-30::CYTH4-GFP*	SC-160 (10), pRF4 (50)
gmEx353	[*grp-1(+); Pdpy-30::NLS::DsRed2*]	bGG836 (10), pRF4 (40), SC73 (50)
gmEx362	*Pmab-5::grp-1::gfp*	SC-79 (10), pRF4 (50), SC73 (50)
gmSi33	*Pmab-5::arf-6::gfp*	# pJT122 (25)
gmSi44	*Punc-86::grp-1::gfp*	# pJT50 (25)
gmSi31	*Punc-86::cnt-2::gfp*	# pJT49 (25)
gmEx393	GRP-1 *Pdpy-30::grp-1::gfp*	SC-94 (10), pRF4 (90)
gmEx428	GRP-1^{K270A} *Pdpy-30::GRP-1^{K270A}::GFP*	SC-128 (10), pRF4 (50)

gmEx440	CC *Pdpy-30::CCgrp-1::gfp*	pAS1 (10), pRF4 (50)
gmEx453	GRP-1^{E155K} *Pdpy-30::grp-1(^{E155K})::gfp*	SC-127 (10), pRF4 (50)
gmEx426	SEC7 *Pdpy-30::SEC7grp-1::gfp*	SC-126 (10), pRF4 (50)
gmEx405	GRP-1^{mutNLS} *Pdpy-30::grp-1^{mutNLS}::gfp*	SC-104 (10), pRF4 (90)
gmEx402	NES-GRP-1 *Pdpy-30::NES-grp-1::gfp*	SC-106 (10), pRF4 (90)
gmEx410	MYR-GRP-1 *Pdpy-30::MYR-grp-1::gfp*	SC-102 (10), pRF4 (90)
gmEx424	MYR-GRP-1^{mutNLS} *Pdpy-30::MYR-grp-1^{mutNLS}::gfp*	SC-116 (1), pRF4 (90)
gmEx460	NLS-mRFP-SEC7 *Pdpy30::NLS-mRFP-SEC7grp-1::GFP*	SC-147 (1), pRF4 (50)
gmEx470	PHPLCd1-mRFP-SEC7 *Pdpy-30::PLCdelta1PH-mRFP-SEC7grp-1-GFP*	SC-159 (1), pRF4 (50)
gmEx458	mRFP-SEC7 *Pdpy-30::mRFP-SEC7grp-1-GFP*	SC-151 (1), pRF4 (50)
gmSi13	EFA-6 *Pmab-5::efa-6::gfp*	# pJT101 (25)
gmSi19	EFA-6^{E447K} *Pmab-5::efa-6E447K::gfp*	# pJT107 (25)
gmSi20	EFA-6$^{\Delta MTR}$ *Pmab-5::efa-6$^{\Delta MTR}$::gfp*	# pJT106 (25)

Part of a DNA injection mix containing coinjection markers and a Mos transposase plasmid as described in the MosSCI transgenesis protocol (FRØKJÆR-JENSEN *et al.* 2008).